

**Polyacrylamide Stiffness-gradient Hydrogels:
A 2D Culture System to Study Cell Mechano-
responsiveness to Substrate Stiffness**

Nuria Barber-Pérez



Master's Thesis

Åbo Akademi University
Master's Degree of Biomedical Imaging

Credits: 45 ECTS

Supervisor: Prof. Johanna Ivaska
Co-supervisor: Camilo Guzmán, PhD

November, 2019

ABSTRACT

ÅBO AKADEMI UNIVERSITY

Faculty of Science and Engineering

NURIA BARBER-PÉREZ

Polyacrylamide Stiffness-gradient Hydrogels: A 2D Culture System to Study Cell Mechano-responsiveness to Substrate Stiffness

Master's thesis, 70 pp

November 2019

Stiffness of the extracellular matrix (ECM) has emerged as a prominent mechanical cue that influences cell behaviour and tissue homeostasis. Importantly, there is growing evidence suggesting that a prolonged dysregulation of the ECM mechanical properties contributes to the development of a permissive pro-invasive tumour microenvironment that favours cancer progression. Polyacrylamide (PA)-based hydrogels are one of the current culture systems to investigate the downstream cellular response to matrix stiffness. However, most of the available protocols for the fabrication of PA hydrogels are limited to uniform stiffness substrates that poorly reproduce the native ECM especially during pathological conditions. In order to mimic the effect of the ECM rigidity on cells, different methods have been developed for the generation of PA-based stiffness gradient hydrogels. However, most of these culture systems are either difficult to reproduce or lack the possibility to determine the stiffness of the gel at specific locations without the need of using atomic force microscopy (AFM).

In the framework of this Master's thesis, a cost-effective and reproducible methodology has been developed for the fabrication of PA-based hydrogels with physiologically relevant stiffness gradients. The hydrogels have been embedded with fluorescently labelled beads and correlation curves between bead density and hydrogel stiffness have been generated, thus allowing the use of bead density as a readout for stiffness and eliminating the need for specialized equipment such as AFM. It has been confirmed that within a 2-60 KPa stiffness range, cancer cells behave as expected, hence demonstrating that these hydrogels can be used as a simple model to dissect different mechano-responsiveness aspects of cells to substrate stiffness.

TABLE OF CONTENTS

ABSTRACT	1
1. INTRODUCTION	3
1.1. Introduction to Mechanobiology	3
1.2. Key players in substrate stiffness mechanosensing	4
1.3. Substrate stiffness in cancer	6
1.4. <i>In vitro</i> hydrogels for mechanobiological studies	8
1.4.1. AFM: an accurate tool to assess mechanical properties of hydrogels	9
1.4.2. Current methods for the fabrication of PA stiffness gradient hydrogels	12
2. MOTIVATION AND AIMS	16
3. MATERIALS AND METHODS	18
3.1. Fabrication of PA bead-containing stiffness gradient hydrogels	18
3.1.1. Fabrication of PA gradient hydrogels with a stiffness range from ~2 KPa to 60 KPa	19
3.1.2. Fabrication of PA gradient hydrogels with a stiffness range from ~0.5 KPa to 22 KPa	22
3.2. Generation of correlation curves between fluorescent beads and stiffness	23
3.2.1. Image acquisition of fluorescent beads	23
3.2.2. Stiffness characterization	24
3.2.3. Image processing and analysis of beads	26
3.2.4. Stiffness data processing and analysis	28
3.2.5. Generation of the correlation curves between beads and stiffness	29
3.3. Validation of the wide-range (2 KPa to 60 KPa) correlation curve	31
3.3.1. Quantitative validation	31
3.3.2. Biological validation	31
4. RESULTS	38
4.1. Fabrication of PA bead-containing stiffness gradient hydrogels	38
4.2. Generation of the correlation curves between fluorescent beads and stiffness	39
4.2.1. Wide-range gradient hydrogel: ~2 KPa to 60 KPa	40
4.2.2. Narrow-range correlation curve: stiffness range from ~0.5 KPa to 22 KPa	43
4.3. Validation of the wide-range (2 KPa to 60 KPa) correlation curve	46
4.3.1. Quantitative validation	46
4.3.2. Biological validation	48
5. DISCUSSION	57
6. CONCLUSIONS	63
6.1. Conclusions	63
6.2. Future work	63
ABBREVIATIONS	64
REFERENCES	65

1. INTRODUCTION

1.1. Introduction to Mechanobiology

Tissues of higher organisms are formed by a mixture of cells and extracellular matrix (ECM). Together, they form a complex, dynamic and highly organized structural and signalling framework that ensures a tight regulation of tissue homeostasis and normal organ function (Alberts et al., 2007; Butcher, Alliston, & Weaver, 2009; Handorf, Zhou, Halanski, & Li, 2015; Paszek et al., 2005). Besides biochemical cues, cells within tissues are constantly exposed to physical cues that they must sense in order to respond and adapt to different mechanical conditions. Tensile forces, compression, physical constraints, shear stress and substrate stiffness belong to the different mechanical forces that can influence cellular fate and cellular central processes such as differentiation, apoptosis, migration and proliferation (Iskratsch, Wolfenson, & Sheetz, 2014). Mechanobiology is a multidisciplinary sub-field of biology that focuses on studying the cellular mechanisms involved in sensing mechanical forces (mechanosensing) and how mechanical cues are translated into readable biochemical signals for the cell, leading to the activation of different signalling pathways and cellular responses (mechanotransduction) (Figure 1; Humphrey, Dufresne, & Schwartz, 2014; Koser et al., 2016; Wang, Tytell, & Ingber, 2009).

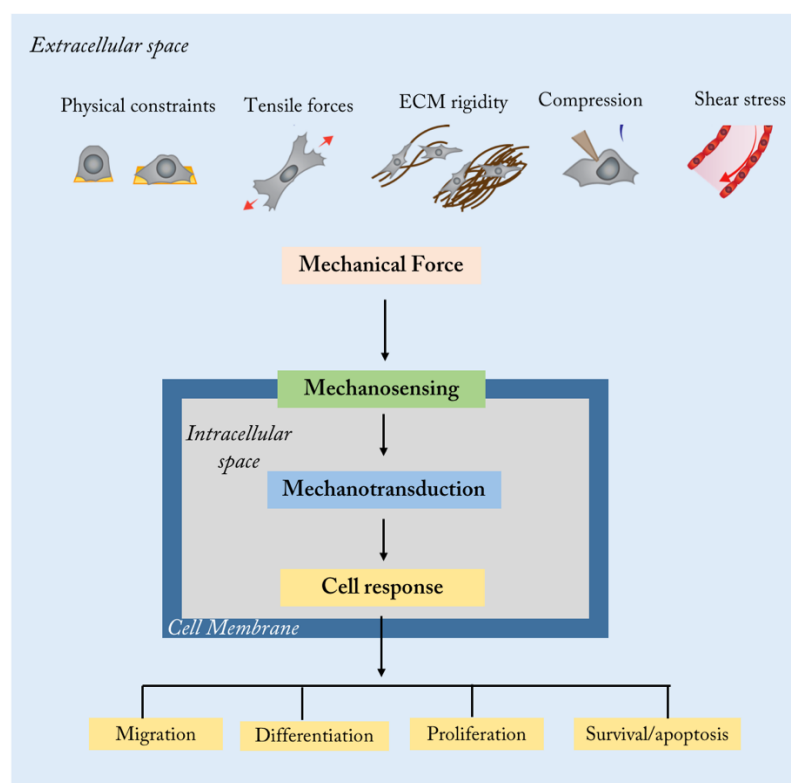


Figure 1. Schematic diagram showing the general flow of mechanobiological events. Cells are exposed to a variety of mechanical forces that they sense through specific cell membrane mechanoreceptors (Mechanosensing). These physical stimuli are converted into a readable format for the cell through the activation of different signalling pathways (Mechanotransduction). Such mechanotransduction results in the modulation of gene and protein expression profiles that lead to different cellular processes and behaviours.

1.2. Key players in substrate stiffness mechanosensing

Among the abovementioned mechanical forces, substrate stiffness has emerged as a critical factor that regulates cell behaviour and is essential for tissue mechanical homeostasis (Acerbi et al., 2015; Cox & Epler, 2011; Discher, Janmey, & Wang, 2005; Paszek et al., 2005; Waterman, 2014; Yeung et al., 2005). The mechanisms through which cells sense mechanical loads, exerted by their local environment, involves constituents of the ECM, cell membrane receptors and intracellular structures (Humphrey et al., 2014; Plotnikov, Pasapera, Sabass, & Waterman, 2012).

The ECM is a dynamic three-dimensional network that surrounds cells providing mechanical support and influencing cellular behaviour through a variety of biochemical and biophysical signals. The stromal ECM is primarily secreted and remodelled by fibroblast and its composition comprises fibrillar proteins (e.g., collagen and elastic fibres), glycosaminoglycans (GAGs) and proteoglycans (PGs). The biggest contribution to substrate stiffness and strength is given by collagen fibre density, orientation and cross-linking (Hay, 2013).

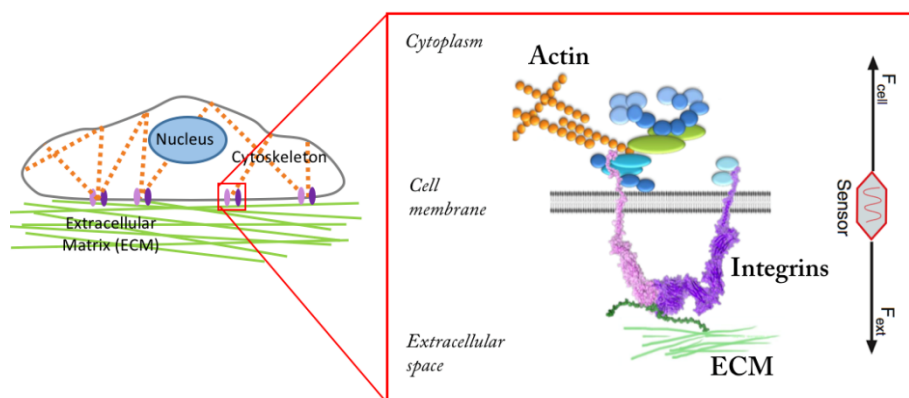


Figure 2. A schematic depicting a cell embedded in ECM and a close-up view of a FA complex showing the key players in cell-matrix interactions: Actin, integrins and ECM. Integrins physically link the ECM to the actin cytoskeleton and function as bidirectional transmembrane sensors that transmits forces from the ECM (outside-in) and to the ECM (inside-out). [Figure modified from (Chen, 2008)]

Mechanosensing of the substrate stiffness is mediated by integrin-based cell-adhesions that physically link the ECM to the intracellular actin cytoskeleton (*Figure 2*; Hamidi & Ivaska, 2018; Horton et al., 2015; Kanchanawong et al., 2010). Integrin-based focal adhesions (FAs) are proposed to work as a force-sensitive molecular clutch that transmits forces from the ECM (outside-in) and to the ECM (inside-out) (Elosegui-Artola et al., 2016). When integrins, the main transmembrane mechanoreceptors, bind to specific proteins of the ECM (e.g., collagen) they undergo conformational changes and become activated (Sun, Guo, & Fässler, 2016). This interaction triggers the recruitment of many cytoskeletal, scaffolding and signalling proteins that accumulate forming nascent adhesion points. Force-induced conformational changes in some of these adhesion-associated proteins (e.g., talin, vinculin, etc.) reveal binding sites for the actin cytoskeleton and other adhesion and signalling components that promote integrin clustering and maturation of FA (Kechagia, Ivaska, & Roca-Cusachs, 2019). Upon high substrate stiffness the number and size of FA as well as actomyosin contractility increase leading to reinforcement of intracellular contractile structures to counterbalance external forces (*Figure 3*; Kass, Epler, Dembo, & Weaver, 2007; Paszek et al., 2005). This structural reorganization of the cytoskeleton and tensional forces at the ECM-integrin-cytoskeleton induce the activation of different downstream signalling pathways, which results in gene expression and determination of the final cellular response (Sun et al., 2016; Vicente-Manzanares, Choi, & Horwitz, 2009; Waterman, 2014).

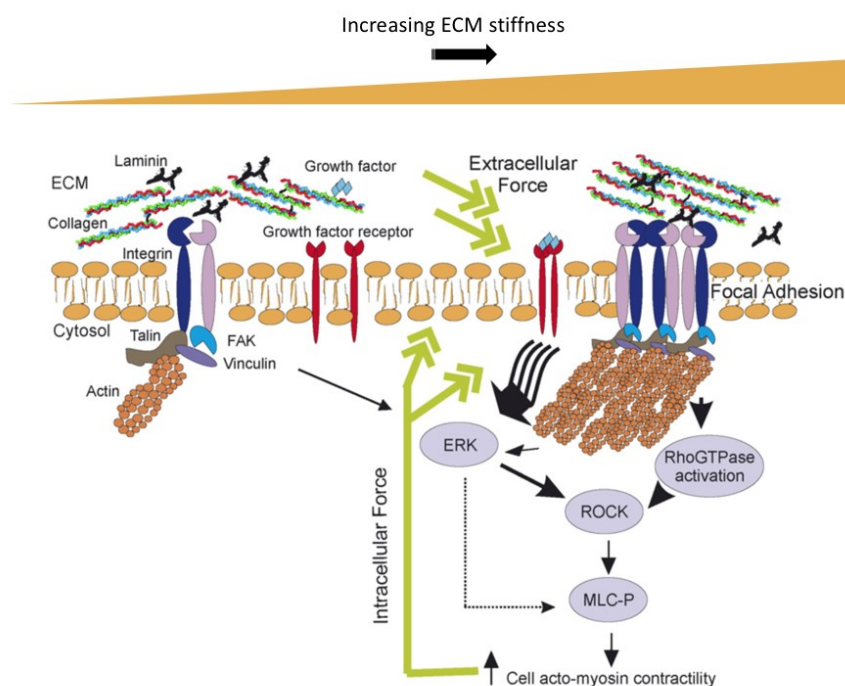


Figure 3. FA maturation mediated by the increase of ECM stiffness. On the left a nascent adhesion, integrins bind to an ECM protein (e.g., collagen) and physically connect to actin through linker proteins (e.g., talin, vinculin). Also, signalling adaptors (e.g., FA kinase (FAC), Src family kinases) are recruited to the adhesion complex. Matrix stiffening favours integrin clustering, FA stabilization and maturation (right) which in turn promotes the Rho/ROCK pathway, actin contractility and cell-generated intracellular forces to the ECM. [Figure modified from (Kass et al., 2007)]

1.3. Substrate stiffness in cancer

Stiffness is defined as the intrinsic resistance of a certain material to an applied force. In mechanobiology it can be used as metric for matrix rigidity and it is reported by the Young or elastic modulus (E) in Pascals (Pa) (Discher et al., 2005). This elastic modulus varies distinctly between and within tissues and it is inherently correlated to their physiological function (*Figure 4*; Butcher et al., 2009). A prolonged deregulation of the ECM stiffness has been associated to an array of pathologies including cancer, fibrosis, muscular dystrophies, aberrant wound healing and aging (Butcher et al., 2009; Cox & Epler, 2011; Handorf et al., 2015; Humphrey et al., 2014).

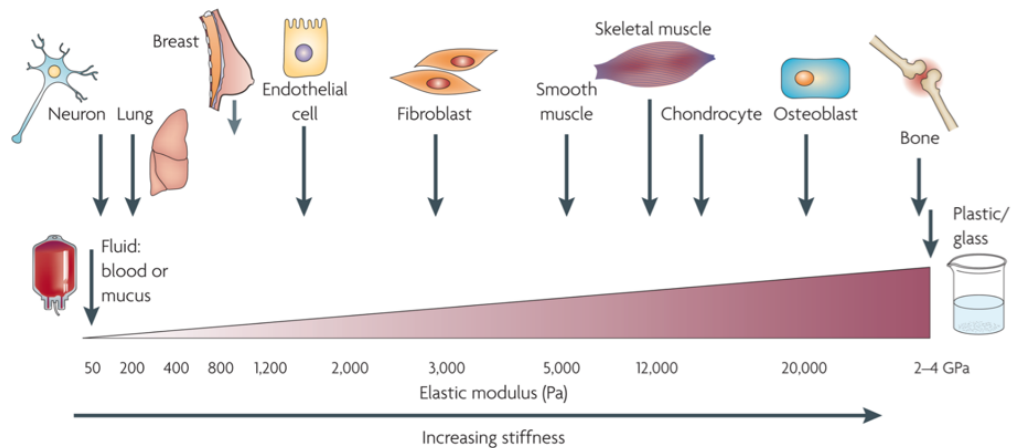


Figure 4. Biomechanical properties of different tissues in terms of stiffness (E), measured in Pa. Each type of cell is exposed to a certain local ECM stiffness which influences cell growth, survival, differentiation, morphogenesis and that is critical for tissue normal function. For instance, neurons are exposed to a highly compliant matrix whereas osteoblasts survival occurs optimally at stiffer matrix. A prolonged alteration of the ECM mechanical properties has been associated to an aberrant cell phenotype and tissue function. [Figure printed from (Butcher et al., 2009)]

Cancer is one of the major causes of death worldwide and, growing evidence suggests that decreased ECM compliance appears to precede cancer development and progression (*Figure 5*; Pickup, Mouw, & Weaver, 2014; Provenzano, Inman, Eliceiri, & Keely, 2009). Cancer cells seem to promote stiffening of their surrounding by an excess of ECM

deposition and cross-linking of pre-existing matrix. This results in a permissive pro-invasive tumour microenvironment that favours cancer migration and invasion (Acerbi et al., 2015; Attieh & Matic, 2016; Butcher et al., 2009; Chin, Xia, Discher, & Janmey, 2016; Cox & Ertler, 2011). Hence, aberrant stiffness of the ECM and the cellular components involved in downstream response to stiffness, could be used as a potential target in drug development and cancer treatment (Lampi & Reinhart-King, 2018; Rehfeldt, Engler, Eckhardt, Ahmed, & Discher, 2007).

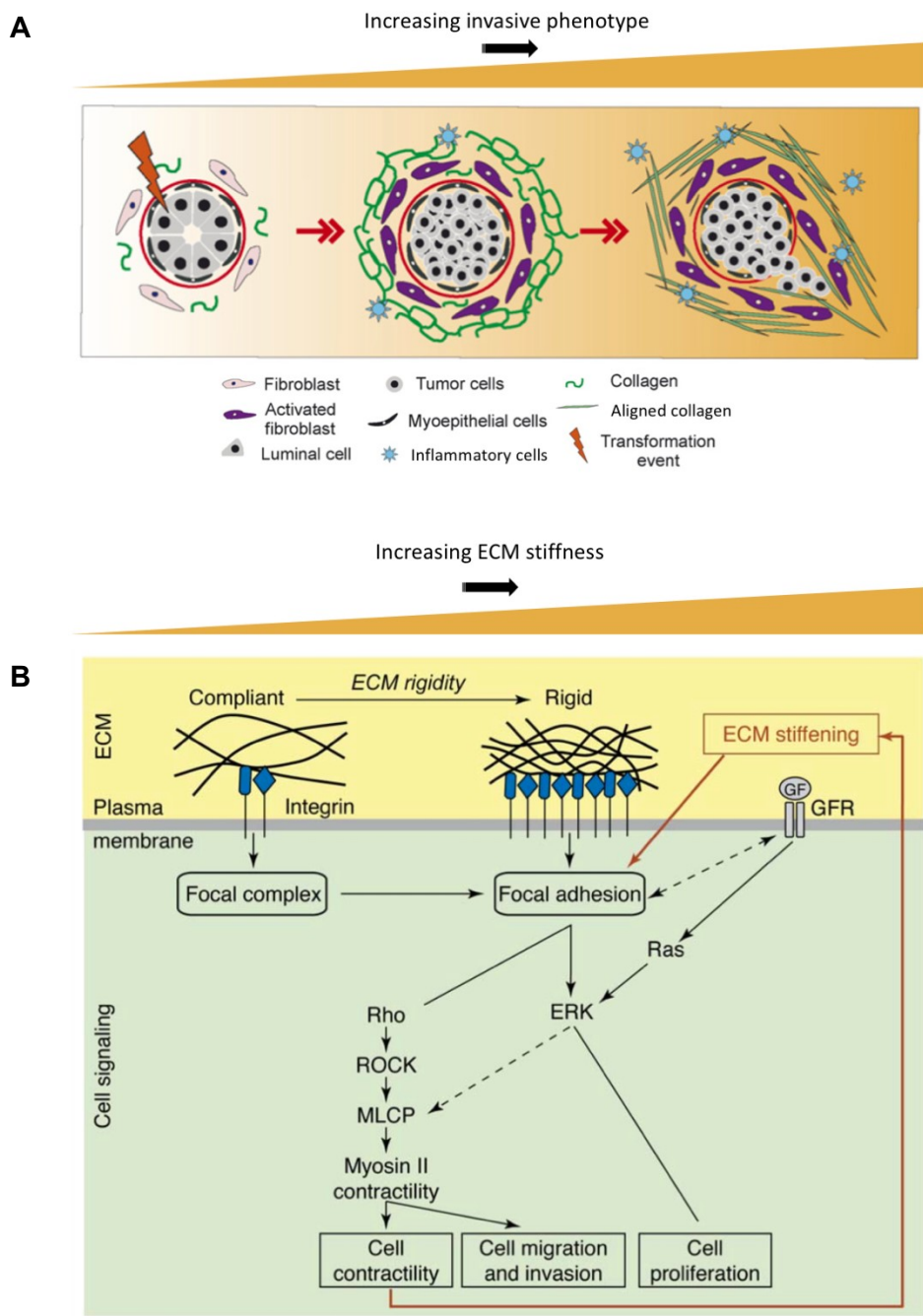


Figure 5. Consequences of increasing ECM rigidity in breast cancer progression and integrin signalling. **A)** Stages of breast tumorigenesis and associated changes within the tissue stroma that promote disruption of mechanical homeostasis and cell conversion towards a malignant

phenotype. From left to right, normal mammary ducts, mammary ductal carcinoma and conversion to a malignant phenotype. The last characterized by increasing matrix deposition and remodelling which contributes to cell migration and invasion. [Figure modified from (Kass et al., 2007)] **B**) Elevated ECM rigidity promotes integrin activation and formation of more numerous and bigger FAs which in turn leads to an increase of cell contractility via Rho/ROCK pathway. Upon transformation events, this positive feedback loop (red arrow) is amplified and contributes to a further ECM stiffening which results in a fibrotic microenvironment that favours cell migration, proliferation and invasion.[Figure modified from (Larsen, Artym, Green, & Yamada, 2006)]

1.4. *In vitro* hydrogels for mechanobiological studies

There is a wide range of available tools to study the impact of intra- and extracellular forces in distinct cellular processes (Iskratsch et al., 2014; Khalili & Ahmad, 2015; Muhamed, Chowdhury, & Maruthamuthu, 2017; Nematbakhsh & Lim, 2015). One of these tools is hydrogels, water-swollen polymer-based networks that try to mimic the native ECM mechanical properties (Caliari & Burdick, 2016). Among other applications (Ahearne, Yang, & Liu, 2008; Xia, Liu, & Yang, 2017), they have been extensively used *in vitro* as cell culture systems to investigate cellular behaviour, including proliferation, differentiation, locomotion, morphology, spreading and adhesion (Discher, Mooney, & Zandstra, 2009; Khatiwala, Peyton, & Putnam, 2006; Rehfeldt et al., 2007; Vining & Mooney, 2017). Hydrogels are broadly classified based on their polymer composition (i.e., natural, synthetic or hybrid) and on their dimensionality (2D or 3D). In addition, a variety of hydrogels can be found in each of these categories and the appropriate selection will depend on the study requirements (Liu & Vunjak-Novakovic, 2016; Wong, Leach, & Brown, 2004).

Among the variety of possible hydrogels, 2D Polyacrylamide (PA) hydrogels have shown to provide a suitable tool for culturing cells and for carrying out basic mechanobiological studies on cell response to substrate stiffness (Kaukonen et al., 2016; Paszek et al., 2005; Tse & Engler, 2010; Yeung et al., 2005). PA hydrogels are made from synthetic chains of acrylamide monomer and bis-acrylamide cross-linker. The reaction between both is called polymerization and it is often carried out by adding ammonium persulfate (APS) which provides free radicals, and tetramethylethylenediamine (TEMED) which serves as initiator of the polymerization reaction. The desired stiffness or cross-link density of the hydrogel can be adjusted by varying the relative concentration of acrylamide/bis-acrylamide. PA hydrogels are usually fabricated on coverslips that have been previously functionalized with aminosilanes (e.g., Plus One Bind Silane solution) to allow the gel coupling. Prior to cell culture, the hydrogel surface needs to be activated

with a cross-linker (e.g., sulfo-SANPAH) to enable protein conjugation (e.g., fibronectin, collagen, etc.) to support cell adhesion (Caliari & Burdick, 2016; Tse & Engler, 2010; Wong et al., 2004).

PA hydrogels have various important advantages for their application in cell culture and studies of cell response to substrate mechanics:

1. The stiffness or E of the hydrogel can be tuned to the desired value by varying the relative concentration of acrylamide and bis-acrylamide.
2. There are well-established fabrication protocols and all components required for the fabrication are available from commercial vendors.
3. They are stable under culture conditions, and the conjugated adhesive ligands for cell adhesion can be controlled. This, together with a finely controlled substrate stiffness, can provide a better understanding of force-dependent cell-substrate interactions.
4. Because PA gels are translucent and thin, immunofluorescence stained cells can be observed at high magnification using standard fluorescent microscopy techniques.

However, PA hydrogels also have some important limitations that impede them from being the preferred method in some mechanobiological studies:

1. Once fabricated, the stiffness of PA hydrogels needs to be assessed. The most appropriated tool to measure stiffness at the micron-scale level is atomic force microscopy (AFM; Caliari & Burdick, 2016; Rehfeldt et al., 2007; Xia et al., 2017).
2. The available fabrication protocols are principally developed to create homogeneous stiffness hydrogels (constant E).

1.4.1. AFM: an accurate tool to assess mechanical properties of hydrogels

AFM belongs to a family of instruments named scanning probe microscopes (SPMs). In contrast to conventional light-based microscopes, this family of instruments do not include optical elements in their design but rather a mechanical probe that is used to “feel” the sample.

The AFM’s basic principle relies on the forces between its probe tip and the sample surface. To measure these forces, AFM uses a mechanical probe consisting of a micro-tip

attached to the free end of a flexible cantilever. The tip is used to raster scan the sample and a laser beam is focused at the back of the cantilever. The nanometric precision that is required to move the probe across the sample is achieved by using piezoelectric scanner and a feedback loop at a constant force. As the cantilever moves, the interaction forces between the tip and the sample produce deflection of the cantilever. The cantilever acts as a transducer of these forces by reflecting the laser beam onto a four-quadrant photodiode detector (*Figure 6*). Based on the position of the laser on the quadrant, the photodiode outputs a different voltage which corresponds with the cantilever deflection. Upon this principle and depending on the AFM operating mode, the cantilever deflection provides information that can be used to produce either a topographic or an elastic map of the sample.

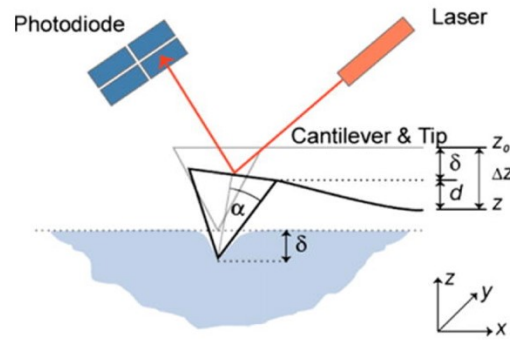


Figure 6. Scheme of AFM's basic principle. [Figure printed from (Rehfeldt et al., 2007)]

In particular, the force spectroscopy mode is perfectly suited to characterize the stiffness or E of a sample to the micron-scale level (Caliari & Burdick, 2016; Engler, Richert, Wong, Picart, & Discher, 2004). In this mode, the AFM-tipped probe is used as a nanoindenter. It is brought into contact with the hydrogel surface and it is pushed into the matrix (Δz) causing the deflection of the cantilever (d). During this process (approaching), a force-distance indentation curve is generated (*Figure 7A*). E is automatically inferred from this curve by fitting the corresponding mathematical model (variant of the Hertz model) which ultimately depends on the shape of the probe tip. For instance, the Young's modulus equation for a pyramidal tip is:

$$E = \frac{\pi (1-\nu^2)F}{\delta^2 2 \tan \alpha},$$

Equation 1. Young's modulus equation for a conical probe tip

where ν is the Poisson ratio of the gel, F is the force extrapolated from the cantilever deflection and spring constant ($F = k_c * d$), δ is the indentation ($\delta = \Delta z - d$) and α is the opening angle of the conical tip (Rehfeldt et al., 2007). The slope of the force-distance curve during indentation provides information of the sample stiffness, where the deflection slope becomes steeper at increasing stiffness (*Figure 7B*). In contrast, during retraction, the curve provides information regarding adhesion forces that may be of interest for other purposes (e.g., molecule fishing).

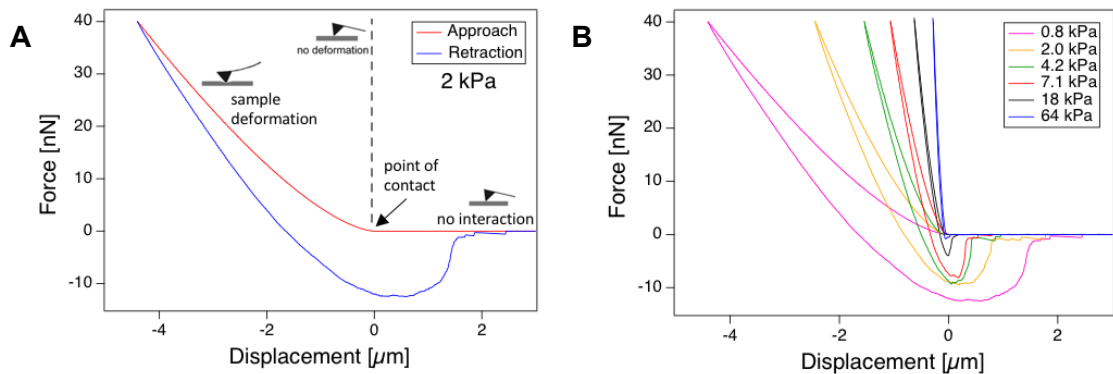


Figure 7. **A)** Force-distance curve depicting the indentation curve (red line) while cantilever approaches and gets in contact with the sample surface and adhesion curve (blue line) while retracting from the sample. **B)** Force-distance indentation curves at increasing sample stiffness. At a constant force, the deflection experimented by the cantilever decreases at increasing stiffness of the sample.

Due to the small size of the probe tip and precise movements of the piezoelectric, the AFM is capable of mapping hydrogel stiffness on the same scale (micron length) as cells can feel their matrices. In addition, the AFM can be operated in liquid, which is a requirement for keeping the hydrogels hydrated during measurements. All in all, the AFM is the most appropriated tool to measure hydrogel stiffness. However, this tool has a few important limitations: (1) it is not commonly accessible to every laboratory, (2) because it works very differently to light-based microscopes, using it properly requires certain knowledge and expertise (JPK instruments, 2012; Neumann, 2008), (3) it is considerably slow and time consuming, both because of the time needed to set it up and the time it takes for the cantilever to indent the sample and to generate the force-distance curve for each measured point.

1.4.2. *Current methods for the fabrication of PA stiffness gradient hydrogels*

Current protocols for the fabrication of PA hydrogels are mostly developed to produce uniform substrate stiffness (constant E). This type of culture systems may be informative to elucidate basic processes involved in cell response to stiffness. However, they fail to mimic the gradient variation of ECM stiffness that also exist *in vivo*, both in physiological and pathological conditions (Xia et al., 2017). For instance, in physiological conditions there are interfaces of variant stiffness between and within tissues that play an important role in cell migration, differentiation and proliferation (Koser et al., 2016; Mao, Shin, & Mooney, 2016; Moffat et al., 2008; Richter, Emadi, Getnick, Quesnel, & Dallos, 2007). Also in pathological conditions, these stiffness gradients are known to importantly influence cellular behaviour and disease progression (e.g., fibrogenesis, tumour metastasis, angiogenesis, durotaxis, etc.; Butcher et al., 2009; Elkrief et al., 2014; Lo, Wang, Dembo, & Wang, 2000; Takuma et al., 2015).

A few methods have been developed to generate PA gradient hydrogels that more closely resemble the stiffness heterogeneity observed *in vivo*. These methods have been divided into two different categories:

1. Hydrogels that do not include an indirect measure as a readout for stiffness, thus they require the use of AFM.

Both, Wong, et al. and Sunyer, et al. (Sunyer, Jin, Nossal, & Sackett, 2012; Wong, Velasco, Rajagopalan, & Pham, 2003), used a photo-polymerization method to fabricate hydrogels with a stiffness gradient. This method includes a photo-activatable compound (e.g., Irgacure 2959) in the acrylamide/bis-acrylamide mixture. The polymerization reaction is initiated by exposing the mixture to ultraviolet (UV) light with the appropriate wavelength. By varying the amount of light to which the mixture is exposed to, different hydrogel stiffness (polymer cross-link density) is achieved. In the method used by Wong, et al., the gradient exposure is achieved by using a variable grey-scale photomask. (*Figure 8A*). In the method used by Sunyer, et al., the gradient exposure is achieved by moving an opaque mask at a constant speed (*Figure 8B*).

The main advantage of these two methods is that the matrix stiffness profile can be controlled by light exposure, hence the gradient area created within the hydrogel is considerably wide and the slope of the gradient curve is shallow. However, there are many parameters that need to be properly adjusted and controlled (e.g., light intensity; light source distance to the gel, exposure time; grayscale of the photomask, etc.) to

achieve the desired gradient. Also, the materials and conditions required to control light exposure are not available to every laboratory.

Lo, et al., on the other hand, used the standard procedure (variation of acrylamide/bis-acrylamide concentration ratios) to prepare two PA pre-mixtures, one soft and one stiff (Lo et al., 2000). The stiffness gradient was created by placing one drop of each pre-mixture (right after adding TEMED and APS) adjacent to each other and dropping on them a cover glass that leads to the mixing and diffusion of both solutions. To distinguish between both regions of the gradient, soft and stiff part, they embedded fluorescent beads in one of the mixture solutions before starting the polymerization reaction (*Figure 8C*).

The main advantage of this method is that there exist well-established protocols to obtain the desired stiffness by modulation of acrylamide/bis-acrylamide concentrations. Also, the method to create the rigidity gradient is quite straightforward, thus it can be easily implemented in any laboratory with usual lab equipment. Furthermore, thanks to the fluorescent beads, it is possible to differentiate between the soft and stiff part of the gel without the need of using AFM. However, compared with the previously described methods, the generated area of gradient within the hydrogel is much narrower, the stiffness gradient profile is less controlled, and the slope of the gradient curve is steeper. Also, Hadden, et.al. applied the common procedure to fabricate PA hydrogels but they used a complex two-layer polymerization method to create the stiffness gradient (*Figure 8D*; Hadden et al., 2017). The obtained gradient has a precise and well-characterized stiffness profile which is displayed within a wide area and with a shallow stiffness curve. However, the resulting gel is too thick to allow the observation of small cellular structures with high-resolution microscopy techniques.

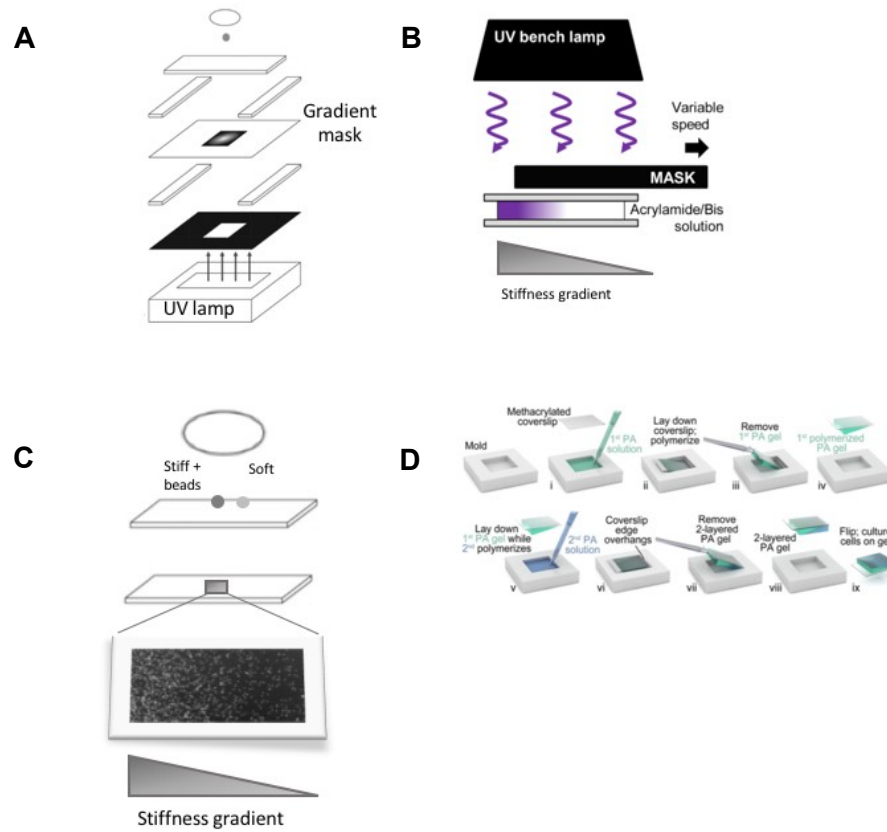


Figure 8. **A)** Photo-polymerization method by gradient photo-mask.[Figure modify from (Tse & Engler, 2010)]; **B)** Photo-polymerization method by opaque mask.[Figure modify from (Sunyer et al., 2012)]; **C)** Mixing and diffusion of different stiffness solutions (stiff solution including fluorescent beads).[Figure modify from (Lo et al., 2000)]; **D)** Two-layer polymerization method.[Figure modify from (Hadden et al., 2017)].

All the above described methodologies, each with their advantages and disadvantages, have achieved the fabrication PA hydrogels with a stiffness gradient. However, they all have an important limitation that needs to be considered. Regardless of knowing the directionality of the gradient within the gel, it is not possible to know the exact stiffness at which seeded cells are exposed to (at a certain location within the gradient) unless using AFM.

2. Hydrogels that provide an indirect measure that can be used as a readout for stiffness without the need of using AFM.

As Lo, et al., Koser, et.al., also prepared two PA pre-mixtures (one soft and one stiff) by using the standard procedure (Koser et al., 2016). However, in this method, a custom-designed chamber was used as a mould to fabricate the gradient hydrogel and instead of tagging one of the pre-mixtures with fluorescent beads, they used

fluorescein. Right after adding the polymerization agents (TEMED and APS), the fluorescently-tagged stiff solution was poured into the chamber (filling half of it). Then the soft solution was poured to fill the rest of the chamber. The mixing and diffusion happened at the interface between both solutions, creating a stiffness and fluorescent gradient. Moreover, they produced a stiffness map of the hydrogel (by using AFM) and quantified the fluorescence intensity at the same locations (*Figure 9*). This allowed them to conclude that there is a strong correlation between substrate stiffness and fluorescence intensity. Therefore, enabling the use of fluorescence intensity as a readout for substrate stiffness without the need of using AFM.

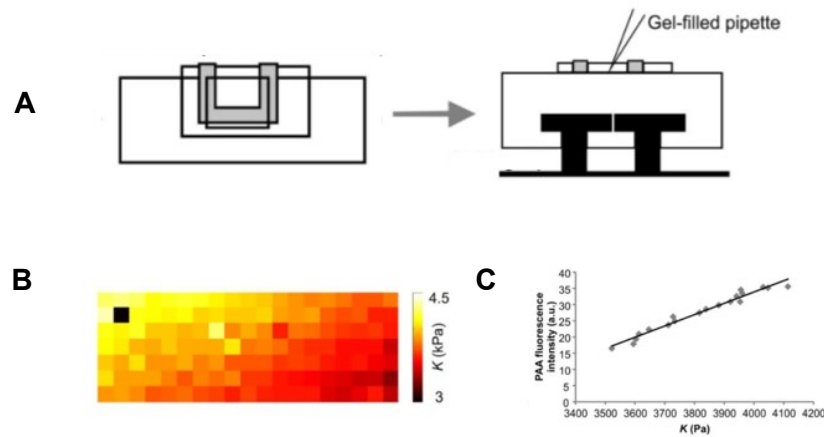


Figure 9. **A)** Custom-designed chamber and filling of the chamber with the two PA solutions, first soft and second stiff tagged with fluorescein, **B)** Hydrogel stiffness map, **C)** Correlation curve between stiffness and fluorescence intensity. [Figure modify from (Koser et al., 2016)]

This method has a very important methodological improvement compared to the previously mentioned methods, as using fluorescence as a readout for stiffness enables to use standard microscopy techniques which are commonly used in every laboratory without the need of using AFM. However, this method also has some disadvantages: 1) due to the mixing technique used to create the gradient, the resulting stiffness profile is less controlled, the gradient area is narrow and the stiffness curve is steep and, 2) the fluorescence intensity can be highly variable depending on the imaging modality used, light setting and bleaching.

2. MOTIVATION AND AIMS

There are different methods for the fabrication of PA stiffness gradient hydrogels. However, most of them are either difficult to reproduce or they require the use of specialized equipment not easily accessible in every laboratory. Moreover, many of these models lack the possibility to know the stiffness to which seeded cells are exposed without the need of using AFM, and they have limitations regarding the ability to image them with high resolution imaging techniques. Hence, it would be beneficial for the research community to either develop a new method, or implement one of the already existing methods, that allows to easily image and quantify cell response to gradient stiffness by using standard microscopy techniques.

To overcome some of the limitations of the currently available methodologies, this project has been divided into three main objectives:

1. To set up a simple, low-cost, robust and time-efficient method for the fabrication of thin PA hydrogels displaying a biologically-relevant stiffness gradient. Additionally, the proposed culture system needs to include another measurable gradient (indirect measure), such as fluorescence, that could correlate with the stiffness gradient. The methodology aims to provide a culture system suitable for high-resolution imaging that more closely resembles the ECM stiffness heterogeneity observed *in vivo*, especially during disease progression (e.g., cancer), for studying cell response to variable stiffness.
2. To determine the correlation, if this exists, between the stiffness gradient and the other measurable gradient, and to generate the best fitting correlation curve between them. The aim is to use the indirect measure as a readout for gel stiffness. This would replace the need of using AFM to determine the stiffness of the gel by more accessible microscopy techniques.
3. To assess the applicability of the proposed hydrogels by performing cancer cell behavioural studies. To do so, HeLa H2B-GFP cells (Human cervical adenocarcinoma cell line expressing H2B tagged with green fluorescent protein) will be cultured on the gradient hydrogels and three known stiffness-sensitive aspects will be studied:

- The subcellular distribution of the well-known mechanotranscription factor YAP/TAZ, and of two other mechano-mediators, Oct-1 and MASTL, that are under investigation in the laboratory where this thesis was conducted.
- Cell morphology: cell total area and circularity
- Number and size of FAs

Figure 10 shows the expected cell response of each stiffness-sensitive aspect under study, depending on the substrate stiffness. When exposed to compact and stiff matrix, characteristic of a permissive tumour microenvironment (reactive stroma), mechanoresponsive regulators (YAP/TAZ; Oct-1 and MASTL) are expected to localize predominantly in the nucleus. In contrast, when cells are exposed to a loose and soft matrix (normal stroma), they are expected to dominate in the cytoplasm (Dupont, 2016; Dupont et al., 2011; Kaukonen et al., 2016; Panciera, Azzolin, Cordenonsi, & Piccolo, 2017). Cell phenotype is also influenced by matrix stiffness, where cells are expected to be more spread and contractile in a stiff matrix, therefore showing a bigger area and forming more and bigger FAs than in a soft matrix (Cox & Epler, 2011; Dupont, 2016; Elosegui-artola et al., 2017; Handorf et al., 2015; Humphrey et al., 2014; Yeung et al., 2005).




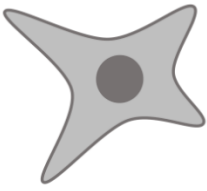

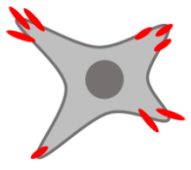
Cell mechanoresponse		NORMAL STROMA Loose and soft ECM	REACTIVE STROMA Compacted and stiff ECM
Nuclear/Cytoplasmic distribution	YAP/TAZ		
	Oct-1		
	MASTL		
Morphology	Cell area		
	Cell circularity		
Focal Adhesions	Number		
	Size		

Figure 10. Expected results for cell mechanoresponse to matrix stiffness.

3. MATERIALS AND METHODS

3.1. Fabrication of PA bead-containing stiffness gradient hydrogels

Prior to the development of this methodology, the different available methods for the fabrication of PA gradient hydrogels (described in section 1.4.2) were evaluated and their applicability considered. Among these, the gradient hydrogel developed by Koser et al., (mixing and diffusion of two solutions in a custom-designed chamber), seemed the most suitable for the laboratory needs and the aims proposed in the current thesis. The method was apparently simple and reproducible with the available equipment in the laboratory and, more importantly, it included an indirect measure which could be used as a readout for stiffness. This method was experimentally tested with a few changes from the original paper. Fluorescein was replaced by fluorescently labelled beads, as it was thought that using density of beads instead of fluorescence intensity would provide a more reliable indirect measure for stiffness. However, it was found that the assembly of the custom-designed chamber was very laborious, the filling of the chamber with PA solutions had many issues and the resulting gel showed very poor reproducibility. For these reasons, this method was discarded.

The new approach that was finally used in the current thesis was an adaptation of the method developed by Lo et al., (mixing and diffusion of two adjacent drops, one soft and one stiff with beads, by covering them with a glass coverslip) but with two significant changes: (1) the mould used for the fabrication of the hydrogel and, (2) the generation of a correlation curve that allows to use the density of fluorescently labelled beads as a readout for stiffness.

Next section describes two protocols for the fabrication of stiffness gradient hydrogels. The first protocol is designed to fabricate gradients whose stiffness spans from 2 KPa to 60 KPa and the second to fabricate gradients whose stiffness spans from 0.5 KPa to 22 KPa. Both protocols were achieved with a trial and error approach until the methodology was robust and reproducible enough.

3.1.1. Fabrication of PA gradient hydrogels with a stiffness range from ~2 KPa to 60 KPa

As a mould to fabricate the PA hydrogel, a 35 mm petri dish (Cellvis, D35-14-1-N) with a 14 mm glass-bottom well (0.13-016 mm thickness) was used. The glass bottom was treated for 20 min at room temperature (RT) with 200 μ l of Bind-silane solution—a mixture of 714 μ l 3-(Trimethoxysilyl)propyl methacrylate (3-TMP, Sigma-Aldrich, M6514), 714 μ l of acetic acid and up to 10 ml of 96% ethanol. This solution was used to covalently attach the PA gel to the glass surface and to avoid its detachment during posterior staining and drying steps. After the Bind-silane was aspirated, the glass was washed twice with ethanol and left to dry completely.

Before the PA pre-mixes were prepared, a reference mark was manually drawn at the bottom of the petri dish, next to the outer right edge of the bottom well (*Figure 11A*). The mark had two purposes: (1) Serve as a reference for placing the PA droplets, soft and stiff, adjacent to each other and (2) Serve as an origin coordinates (x:0, y:0) to locate the gradient region within the gel when imaging the beads. Since spinning-disk confocal microscopy (SDCM) and the AFM are not integrated devices, knowing the coordinates of the imaged region with the SDCM allowed to find the same region at the AFM later on.

Two PA pre-mix solutions, one soft (~ 2 KPa) and one stiff (~ 60 KPa), were prepared to create a gradient of rigidity spanning from 2 KPa to 60 KPa. The desired E of the pre-mixes was adjusted by mixing pre-defined ratios of 40% (w/v) acrylamide monomer (Sigma-Aldrich, A4058) and 2% (w/v) N, N methyl-bis-acrylamide cross-linker (Sigma-Aldrich, M1533) in phosphate-buffered saline (PBS) (*Table 1*). A standard volume (1.7 μ l, 3.6×10^{10} beads/ μ l) of fluorescently labelled (505/515 nm) beads (0.1- μ m carboxylated FluoSpheres; ThermoFisher, F8803) was sonicated during 3 min and added into the stiff pre-mix. Both PA pre-mix solutions, soft and stiff, were briefly vortexed and kept on ice to avoid fast polymerization in later steps (*Figure 11B*).

Polymerization of the soft pre-mix was started by addition of 5 μ l 10% ammonium persulphate (APS; BioRad) and 1 μ l N, N, N', N'-tetramethylethylenediamine (TEMED; Sigma, T-9281) to the solution. The polymerizing soft mixture was quickly vortexed and 7.8 μ l droplet of the solution was pipetted on top of the glass-bottom well, approximately 3 mm from and 1 mm above the reference mark (*Figure 11C*). The same polymerization procedure, addition of 5 μ l of 10% APS and 1 μ l of TEMED, was

followed to initiate the polymerization of the stiff pre-mix (*Figure 11D*). The mixture was quickly vortex and 7.8 μl droplet of the solution was placed approximately 2 mm bellow the soft droplet. A circular coverslip (13 mm) was then placed on top of the droplets by gently dropping it from the reference mark edge towards the opposite side of the glass well. Because the droplets were still in a liquid phase, dropping a coverslip on top of them led to the mixing and diffusion of both solutions across the dish.

Table 1. Relative acrylamide and bis-acrylamide concentrations for the fabrication of uniform (constant E) hydrogels and expected E after polymerization ^a

Acrylamide %	Bis-acrylamide %	40% Acrylamide (μl)	2% Bis-acrylamide (μl)	PBS (μl)	$E \pm \sigma$ (KPa)
5	0.04	63	10	397	0.5 ± 0.4
5	0.07	63	17.5	365	1.8 ± 2
12	0.2	150	50	300	21 ± 1
18	0.4	225	100	175	60 ± 2

^a The values shown in this table were provided by the laboratory which already had well established protocols for the fabrication of uniform PA hydrogels.

The gel was left to polymerize during 1 hour at RT. Upon polymerization the gel was covered with PBS for 5 min before the coverslip was carefully removed with a bent needle. The obtained hydrogel showed a gradient of beads where the region with lower density of beads was expected to correspond to the softest rigidity (~ 2 KPa), the region with higher density of beads was expected to correspond to the stiffest rigidity (~ 60 KPa) and the region in between was expected to contain intermediate values of rigidity within this range (*Figure 11E*).

As a last step the hydrogel was washed once with PBS to remove any left unpolymerized PA. To keep it hydrated, it was completely covered with PBS and stored at 4 $^{\circ}\text{C}$ until used.

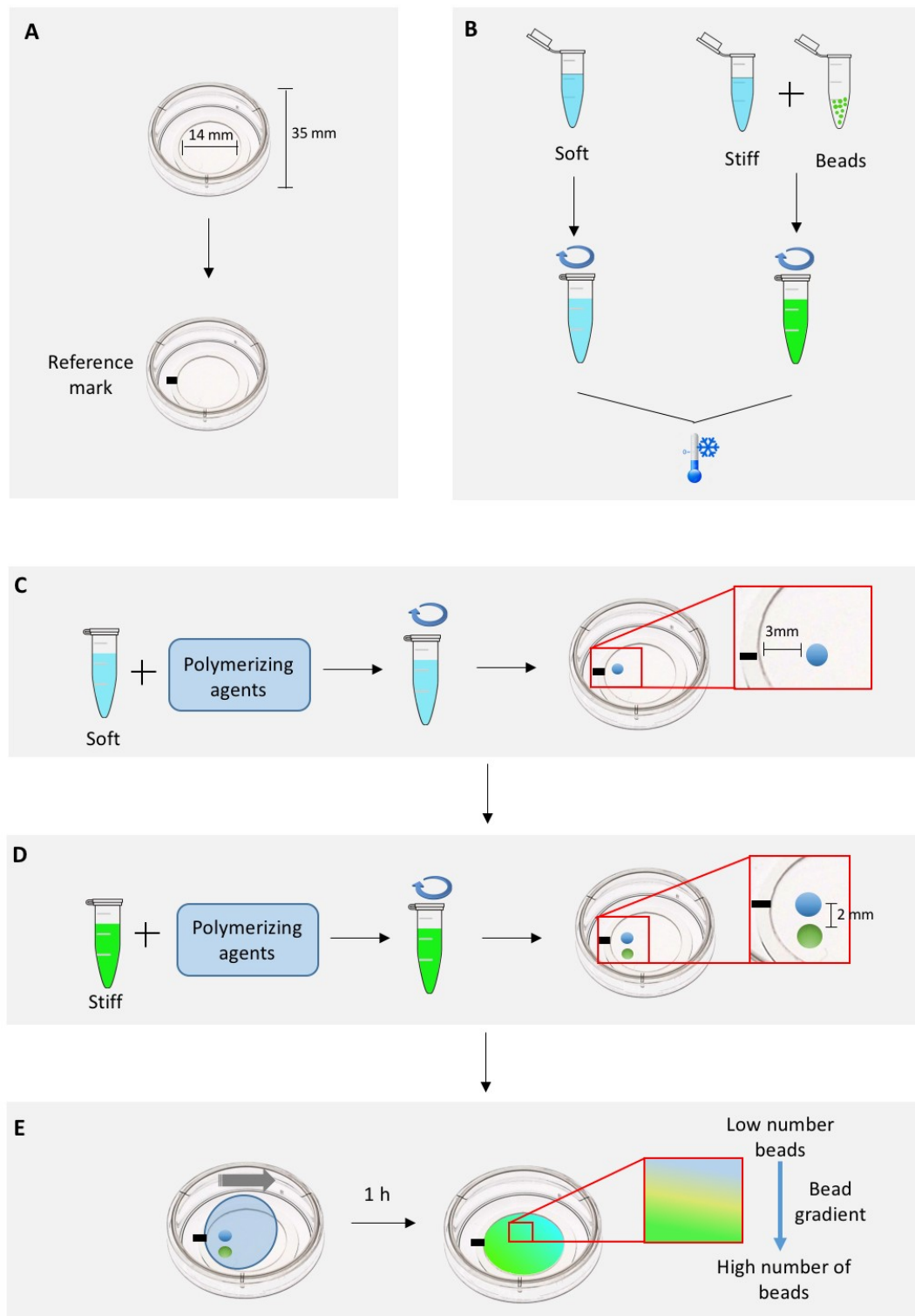


Figure 11. Scheme for the fabrication of PA gradient hydrogels. (A) Glass-bottom petri dish used as a mould for the hydrogel fabrication and location of the reference mark. (B) Soft and stiff pre-mixes prepared by mixing the corresponding concentration of acrylamide and bis-acrylamide. Incorporation of beads in the stiff pre-mix. Vortexing and storage in ice of both pre-mixes before initiating polymerization. (C) Addition of polymerizing agents (APS and TEMED) into the soft pre-mix and location of the pipetted droplet within the glass-bottom well. (D) Addition of polymerizing agents into the stiff pre-mix and location of the pipetted droplet. (E) Mode of dropping the thin coverslip to allow mixing and diffusion of the droplets and region with bead gradient within the gel after 1 hour of polymerization and removal of the coverslip.

3.1.2. Fabrication of PA gradient hydrogels with a stiffness range from ~0.5 KPa to 22 KPa

The fabrication of PA gradient hydrogels with a stiffness range from ~ 0.5 KPa to 22 KPa arose from the need to create a softer stiffness gradient that was more relevant to study mechanoresponse of HeLa cells. In addition, a change was introduced that was expected to improve the quality of the method described in section 3.1.1.

In this case, a 35 mm petri dish with a gridded glass-bottom well (Cellvis, D35-14-1.5GO) was used as a mould to fabricate the gel. Each square of the grid included a letter and a number (*Figure 12*). The incorporation of the new mould aimed to facilitate the localization of the same gel area under both microscopes (SDCM and AFM) used in later steps of the methodology. Therefore, in this case the reference mark was only used as a reference to place the PA droplets and it was no longer used as a reference to locate the gradient within the gel.

For the hydrogel fabrication (0.5 KPa to 22 KPa), PA pre-mix solutions corresponding to 0.5 KPa and 22 KPa were prepared (*Table 1*). The rest of the fabrication steps were performed as described in section 3.1.1. (*Figure 11*).

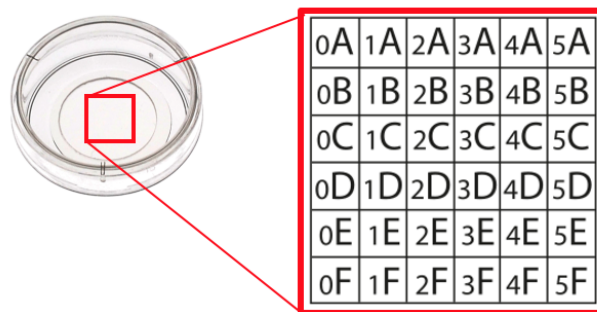


Figure 12. Petri dish with a gridded glass-bottom well.

3.2. Generation of correlation curves between fluorescent beads and stiffness

The next steps of the methodology aimed to verify if the fabricated hydrogels displayed the expected stiffness gradient. Also, to characterize the stiffness and number of beads in order to determine the correlation between both measurements and to generate the corresponding correlation curves. *Diagram 1* shows the workflow followed to achieve the generation of two correlations curves: a wide-range correlation curve (~ 2 to 60 KPa) and a narrow-range correlation curve (~ 0.5 to 22 KPa).

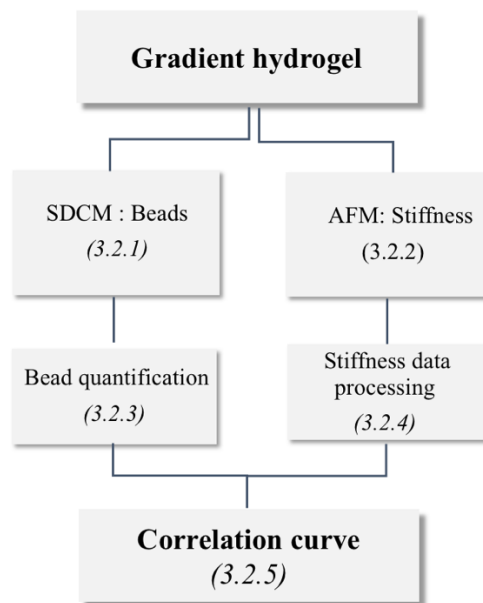


Diagram 1. Workflow scheme for the generation of the correlation curves

3.2.1. Image acquisition of fluorescent beads

Image acquisition of the beads was done with 3i (Intelligent Imaging Innovations) Marianas SDCM (3i CSU-W1, Zeiss), equipped with a 40X objective lens (C-Apochromat 40X/1.1 NA; Zeiss) and sCMOS (Hamamatsu Orca Flash 4; Hamamatsu Photonics) camera. The decision to use this microscope was based on its fast Z-stack acquisition together with its tile options, which facilitates the collection of large data sets.

A visual inspection under the microscope was required to identify a region with a good gradient of beads within the hydrogel. Once located, a tile scan of 12(X) x 12(Y) x 6(Z) images, covering an area of 4 mm x 4 mm was acquired (488 nm laser line, intensity: 800 W/cm²; GFP 510/540 emission filter) (*Figure 13A*). The Z upper limit for the automatic acquisition of each stack was set 1 μ m underneath the gel surface to avoid capturing any

imperfection from the upper layer of the gel. The automatic image acquisition resulted in a total of 144 stacks, each of them of $324.48 \mu\text{m} \times 324.48 \mu\text{m} \times 7 \mu\text{m}$ in size.

Depending on the type of petri dish used as a mould to fabricate the hydrogel, two different approaches were used in order to identify the same region under both microscopes (SDCM and AFM):

- For the wide-range hydrogel ($\sim 2 \text{ KPa}$ to 60 KPa), fabricated on a petri dish without gridded glass-bottom, the X and Y coordinates of the acquired region of interest (ROI) were annotated. The origin of the coordinates was the petri dish reference mark.
- For the narrow-range hydrogel ($\sim 0.5 \text{ KPa}$ to 22 KPa), fabricated on a petri dish with a labelled gridded glass-bottom, the focal plane of the microscope was changed to focus on the grid and a tile scan of bright-field images ($12(X) \times 12(Y)$) was acquired, covering the same region as the beads (*Figure 13B*).

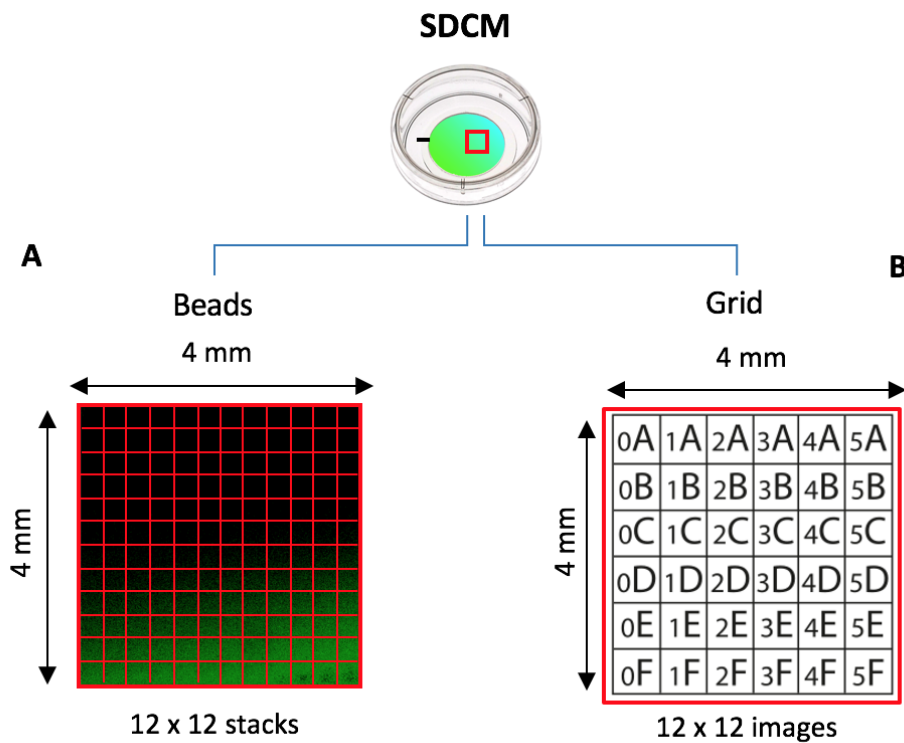


Figure 13. A) Tile scan montage of the hydrogel ROI (4 mm X 4 mm) containing the beads B) Tile scan representation of the glass-bottom grid acquired for the same ROI.

3.2.2. Stiffness characterization

Hydrogel stiffness was assessed using an AFM (NanoWizard) with a CellHesion module (JPK instruments) mounted on a confocal microscope (LSM510, Carl Zeiss Microscopy).

Silicon nitride AFM probes with 1 N m^{-1} (spring constant) cantilever and spherical $10 \text{ }\mu\text{m}$ (diameter) polystyrene particle tip (Novascan Technologies) were used on spectroscopy force measurements where the E was measured. Before carrying out the measurements, the cantilever spring constant and deflection sensitivity were calibrated via the thermal noise method (Hutter & Bechhoefer, 1993). The hydrogels were kept in PBS during the force measurements.

Prior to the distance force measurements, the ROI ($4 \times 4 \text{ mm}$ region of beads previously acquired at the SDCM) was located. Depending on the type of petri dish (with or without grid) two approaches were used:

- For the wide-range hydrogel, the previously annotated X and Y coordinates were located using the manual knobs of the AFM stage. Force measurements were carried out at different location (0.5 mm apart in X and Y coordinates when possible), covering the same region as previously imaged with the SDCM.
- For the narrow-range hydrogel, a CCD (charge-coupled device camera) mounted on the AFM was used to visualize the grid of the petri dish and to locate the ROI within the hydrogel. Force measurements were taken at constant distance (0.5 mm apart in X and Y coordinates when possible) and the letter and number corresponding to these locations were annotated.

In both cases, 9 indentations distributed in a 3×3 points grid ($30 \text{ }\mu\text{m} \times 30 \text{ }\mu\text{m}$) were carried out at each location (9×9 locations) covering the ROI (*Figure 14*). Probe extension was performed by using the following settings: speed $1.5 \text{ }\mu\text{m/s}$, travelling distance $15 \text{ }\mu\text{m}$ and indenting force 40 nN . E for the force distance curves was obtained through JPK data processing software (JPK DP version 4.2) assuming a Hertz model of impact (Hertz, 1881).

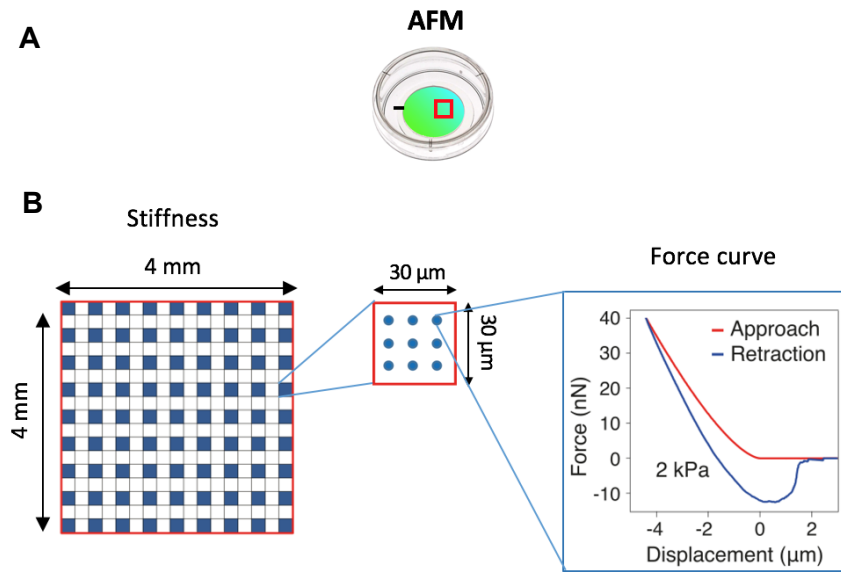


Figure 14. Hydrogel stiffness characterization. **A)** Stiffness characterization at 81 locations of the hydrogel ROI and close view of the 9x9 indentations at each location (30 μm x 30 μm). **B)** Example of the force curve obtained from one indentation.

3.2.3. Image processing and analysis of beads

The images of beads were processed with a custom macro script in Fiji image processing software (Schindelin et al., 2012). The semi-automatic script performed a batch processing of all images acquired for one gel by doing the following steps (*Figure 15A*):

1. Maximum intensity projection of each stack (144 stacks).
2. Bead segmentation of each projected stack based on the threshold input value. The threshold value was chosen by visual inspection of the segmented beads and it could vary considerably between different gels.
3. Division of each image into a 2 x 2 (162.24 μm x 162.24 μm) grid of images, a total of 576 images from the original 144 stacks. This allowed to increase the resolution of the bead quantification. This was especially important in images that displayed a high gradient across them.
4. Quantification of the number of segmented objects (beads), in each image of the grid, with a minimum size of a detected object equal or bigger than 3 pixels. The size limitation was included to avoid the quantification of noise in the analysis which could lead to an overestimation of the bead number.
5. Generation of a .csv file containing the number of beads of each image (split into 4 values corresponding to the 2 x 2 grid) in a column-like format. Additionally,

the script saved 12 segmented images (one image per row from the entire ROI) which allowed the evaluation of the threshold performance.

In the wide-range hydrogel, a single threshold value was used to segment all images of the ROI. In contrast, for the narrow-range hydrogel, different threshold values (approximately 4 per ROI) were used according to the density of beads. This aimed to improve the bead quantification accuracy as a unique threshold seemed not to be appropriate for all the images in the ROI.

The generated .csv file was then processed with a custom Python script that performed the following steps (*Figure 15B*):

1. Calculation of the density of beads per area unit ($1/10^4 \mu\text{m}^2$) for each value of beads contained in the .csv file. The reason to express the beads as density instead of as number of beads was to provide a more standard unit that does not depend on the image size.
2. Generation of an .xlsx file containing a 2D matrix of 24 x 24 values with the spatial distribution of the bead density. The purpose of generating this matrix was to be able to correlate the density of beads and the stiffness at the same ROI location in later steps.

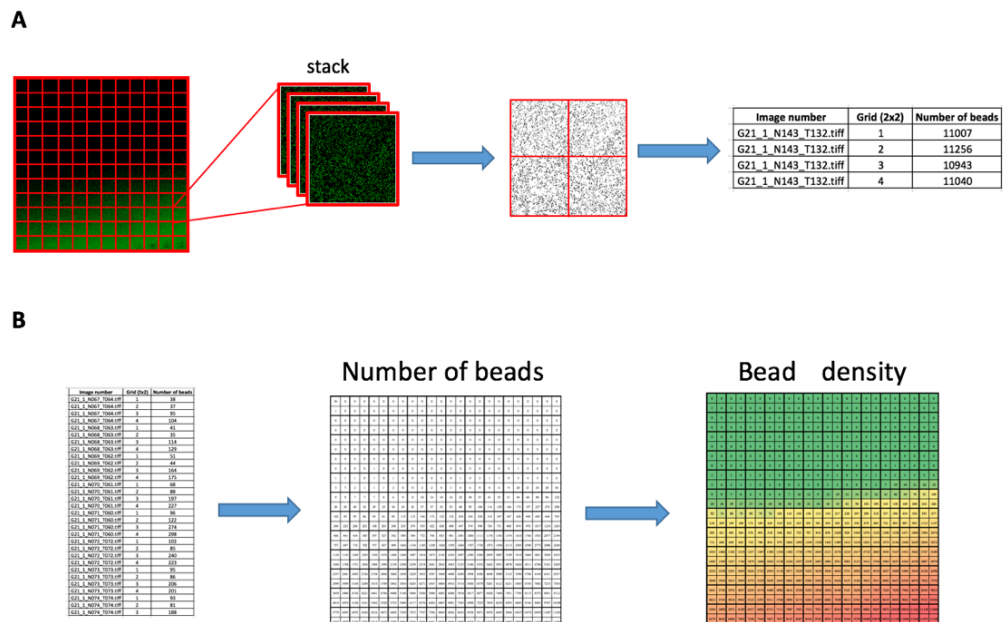


Figure 15. Bead Image processing. **A**) From left to right: (1) maximum intensity projection of one stack, (2) segmentation of beads and division of the projected image into a 2x2 grid of images, and (3) quantification of beads in each image **B**) From left to right: (1) example of generated .csv file containing the number of beads for all the images forming the ROI, (2) number of beads transformed into a 2D matrix format and (3) 2D matrix of the bead density distribution.

3.2.4. Stiffness data processing and analysis

Stiffness measurements from the AFM were processed as following (Figure 16):

1. The 9 stiffness values (E) obtained at each location across the ROI had been generated in separated files. A custom Python script was developed in order to consolidate this data in a single .xlsx file.
2. The mean (M) and standard error (SE) of the 9 stiffness values was calculated for each location.
3. A 2D matrix of approximately 9 x 9 values with the stiffness (mean stiffness at each location) spatial distribution was created.

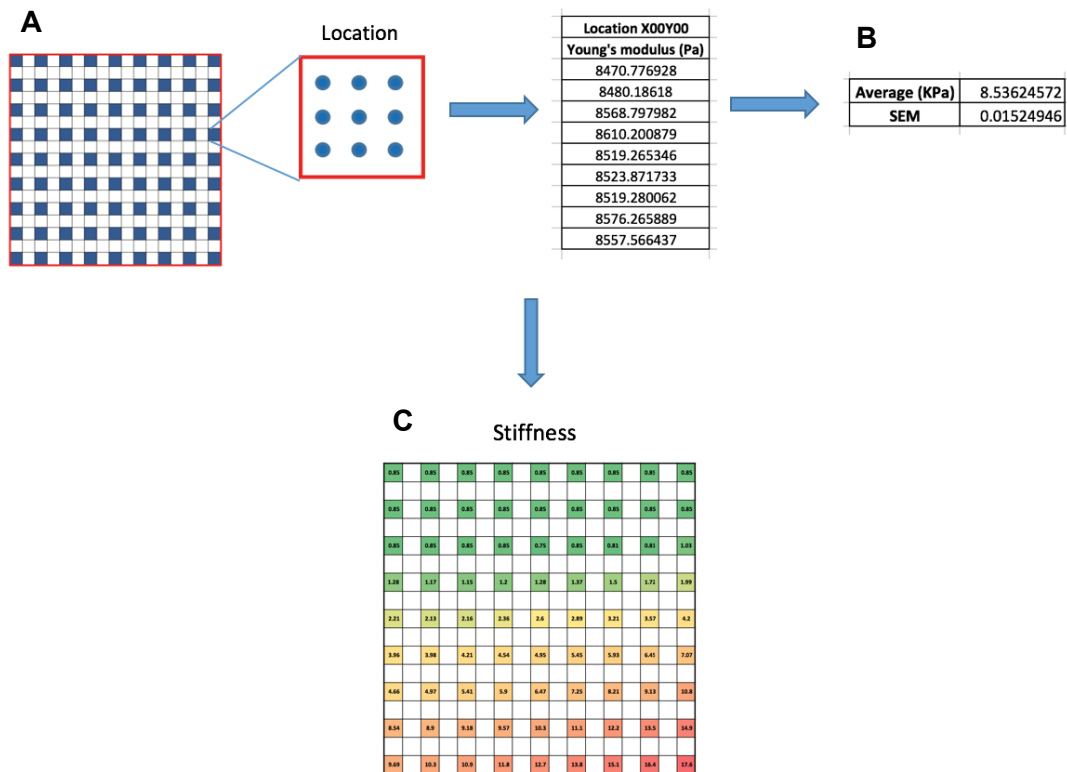


Figure 16. Stiffness data processing. **A)** Example of stiffness measurements at one location of the total ROI. 9 stiffness values obtained from 9 force measurements at one location. **B)** Averaged stiffness at one location. **C)** 2D matrix with the averaged stiffness spatial distribution.

3.2.5. *Generation of the correlation curves between beads and stiffness*

Last part of the methodology was to correlate both measurements, bead density and the stiffness. To do so, it was necessary to first identify the beads location corresponding to the same point where the stiffness measurements were taken. The 2D matrices (bead density matrix and stiffness averaged matrix) previously obtained were used for this purpose. Even though the matrix of beads contained the bead density values for the entire ROI, only those values falling in the same location where the stiffness was measured were used for the correlation curve. Two different approaches were used depending on the hydrogel type:

- For the wide-range hydrogel, the stiffness location was identified within the bead density matrix by measuring the distance where the stiffness had been measured at the AFM (0.5 mm apart in X and Y coordinates when possible). The 4 closest bead density values corresponding to each of these locations were averaged and the SE calculated. The reason for using the mean of the 4 closest values instead of only the single closest value was that the AFM operates at the nanometric level and it is very accurate, but the matrix of beads was not obtained with the same level of accuracy. Missing the exact corresponding location at the bead density matrix could lead to very different results. Therefore, averaging was done to minimize location errors.
- For the narrow-range hydrogel, the glass-bottom grid had been used as a reference to take the AFM measurements. Therefore, it was known which square within the grid (letter and number) each stiffness measurement had been taken from. In this case, the tile scan of the grid images that had been obtained with the SDCM, were overlaid with the bead density matrix. By doing this, it was possible to identify the bead location corresponding to the point where the stiffness measurements were taken (*Figure 17*). As in the wide-range hydrogel, the 4 closest bead density values were averaged at each location to minimize the error. Since the labelled grid resolution was not as high as needed for the AFM precision, this methodology does not reduce the number of images used to calculate the average of beads. However, it is a more robust methodology than the one used before and is less prone to human error.

Igor Pro software (IgorPro 6.37; Wavemetrics) was then used to plot the bead density against the stiffness and to calculate the best fitting curve to the data (*Figure 18*). In both

cases, wide range (~2 to 60 KPa) and narrow range (~0.5 to 22 KPa), the data from three independent hydrogels (n=3) was processed as previously described and combined to generate the two final correlation curves.

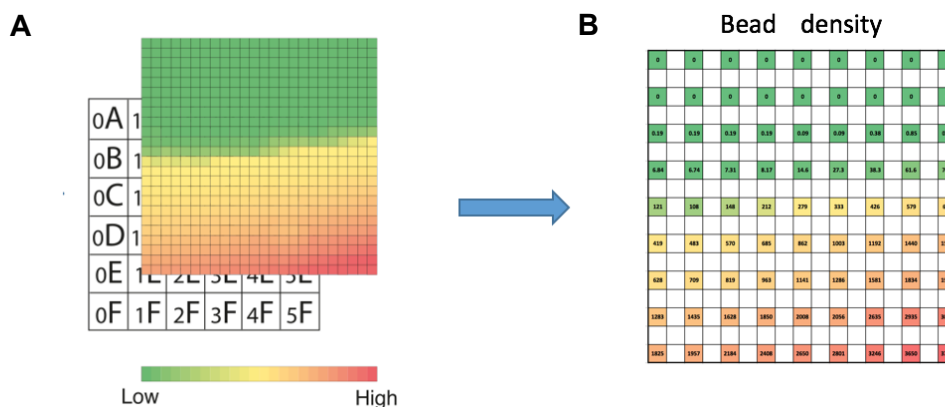


Figure 17. **A)** Overlay of the glass-bottom grid and the bead density matrix. **B)** 2D matrix of averaged bead density at corresponding locations of measured stiffness.

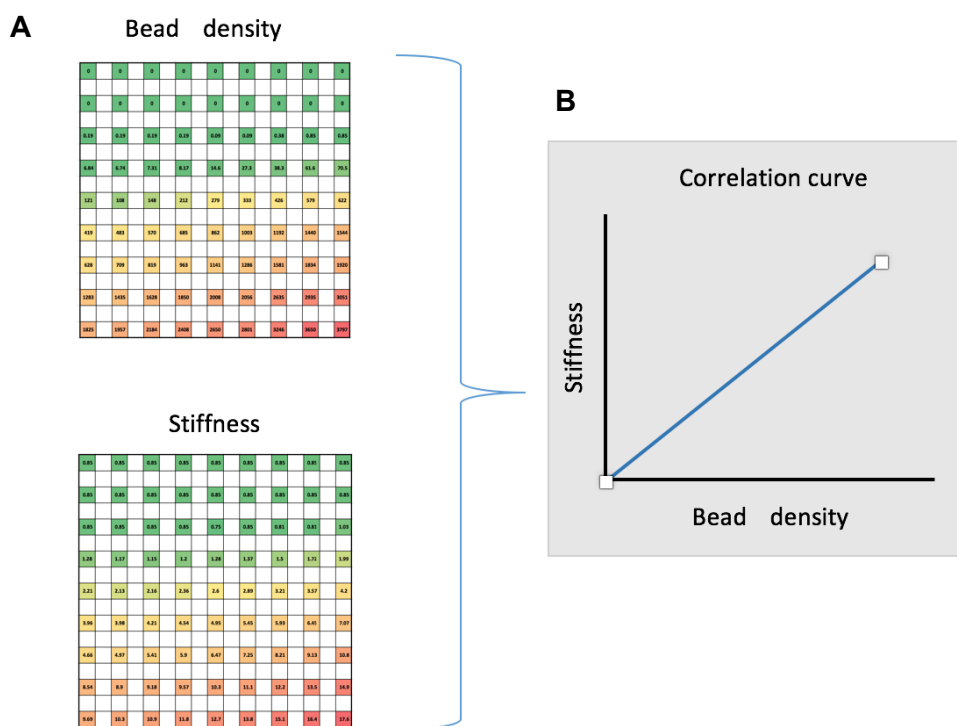


Figure 18. Scheme for the generation of the correlation curves. **A)** 2D matrices of bead density and stiffness. **B)** Plot of the bead density data against the stiffness data at corresponding locations.

3.3. Validation of the wide-range (2 KPa to 60 KPa) correlation curve

3.3.1. Quantitative validation

An extra hydrogel was fabricated to validate the wide-range (2 KPa to 60 KPa) correlation curve obtained from the method described in the previous section (3.1.1). To do so, the beads from a ROI within the hydrogel were imaged, quantified and the density of beads per area ($1/10^4 \mu\text{m}^2$) was calculated. The wide-range correlation curve obtained in section 3.2.5 was used to infer the stiffness by inserting the known bead density in the equation. The real stiffness (“ground truth”) was then measured with the AFM at random location within the ROI. Finally, the SE of the curve was determined by comparing the calculated stiffness values from the equation with the stiffness real values measured at the AFM (Figure 19).

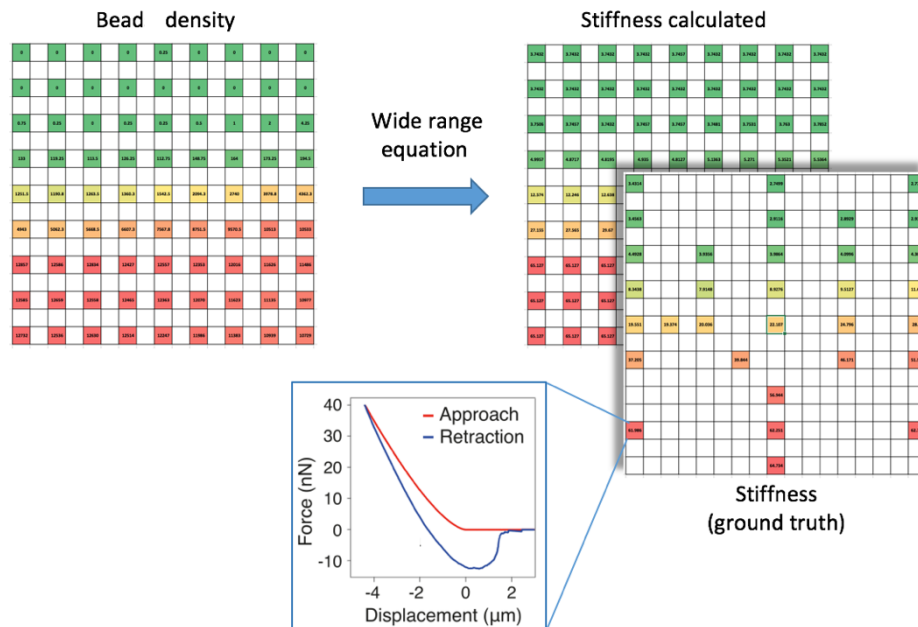


Figure 9

Figure 19. Scheme for the quantitative validation of the wide-range equation

3.3.2. Biological validation

To validate the biological usability of wide-range hydrogels (2 KPa to 60 KPa), HeLa H2B-GFP cells were plated on the gels and their mechano-responsiveness to substrate stiffness was evaluated. Three main aspects of cells were studied:

1. Nuclear to cytoplasmic intensity ratio of mechanoresponsive proteins (YAP/TAZ, Oct1 and MASTL).

2. Cell area and circularity.
3. Visual assessment of FAs quantity and size.

Fabrication and coating of gradient hydrogels

The fabrication of wide-range hydrogels was done as described in section 3.1.1. Before plating the cells on the hydrogels and in order to allow their adhesion to the gel surface, the hydrogels were functionalized, activated and coated.

For functionalization, 0.2 mg/ml of Sulfo-SANPAH (Thermo Scientific, 22589) and 2 mg/ml of EDC (N-(3-Dimethylaminopropyl)-N'-ethylcarbodiimide hydrochloride; Sigma, 03450) in 50 mM HEPES were added on top of the formed gels and they were incubated for 30 min at RT with gentle agitation. Gels were put into a UV-chamber for 10 min without cover to activate the Sulfo-SANPAH and finally washed three times with PBS. Prior to cell seeding, hydrogels were coated overnight at 4°C with a solution of fibronectin (2.5 µg/ml) and collagen I (2.5 µg/ml).

Nine wide-range gradient hydrogels were fabricated to study HeLa H2B-GFP cells, three for each mechanoresponsive protein (YAP/TAZ, Oct 1 and MASTL), cell area and circularity. Additionally, another three gradient hydrogels were fabricated to visually assess the amount and size of FAs formed by HeLa cells.

Cell culture and seeding

HeLa H2B- GFP cells were grown in high glucose Dulbecco's Modified Eagle Medium (DMEM) supplemented with 10% Fetal Bovine Serum (FBS), 1% non-essential amino acids, 1% 2 mM L-glutamine and 1% Penicillin-Streptomycin (Pen-Strep). All the cell culture procedures were carried out in standard aseptic conditions and cells were routinely tested for mycoplasma contamination.

HeLa cells were cultured in sterile petri dishes (150 mm x 15 mm; Sigma-Aldrich) and grown under incubation standard conditions (37 °C, 5% CO₂, 95% humidity). Seeding on the fabricated hydrogels was carried out when cell confluence was approximately of 80%. Prior to plating the cells, the hydrogel coating solution was removed, gels were washed with PBS and covered with 1.5 ml of warm culture medium. Cells were detached from the petri dishes with 1xTrypsin and 15.000 to 20.000 cells/ml of culture medium were seeded for 24h on pre-coated gradient hydrogels.

Immunofluorescence

Cells were fixed with warm 4% PFA added straight into the media (i.e., 1/3 of the total culture volume from 16% PFA stock) at RT. Blocking and permeabilization was done with 0.3% Triton-X in 10% horse serum for 15 min. After washing with PBS, cells were incubated overnight at + 4 °C with one of the following primary antibodies: mouse anti-YAP/TAZ (1:75); rabbit anti- Oct1 (1:75); rabbit anti-MASTL (1:100); or mouse anti-Paxillin in 10% horse serum. Next, cells were washed with PBS and incubated 1h and 30min at RT with AlexaFluor 647-conjugated secondary antibody (1:400) and Phalloidin Atto 425 (1:75). Finally, cells were washed and kept in PBS until imaged.

Microscopy

HeLa cells and beads were imaged with 3i (Intelligent Imaging Innovations) Marianas SDCM (Zeiss), equipped with a 40X objective lens (C-Apochromat 40X/1.1 NA; Zeiss) and sCMOS (Hamamatsu Orca Flash 4; Hamamatsu Photonics) camera.

Initially, cells were imaged at different locations across the gradient of beads expecting to see progressive changes in cell mechanoresponsive phenotype. However, it was observed that changes in cell phenotype happened already where a few beads were present (~ 6 to 7 KPa). This indicated that the majority of the hydrogel gradient contained cells expressed a stiff phenotype and only those located where no beads were present (≥ 2 KPa) showed a different phenotype (*Figure 20*). For this reason, it was decided to avoid imaging cells located at intermediate location of the gradient and only cells located at both extremes of the hydrogel, the softest part of the gradient (no beads) and at the stiffest part of the gradient (high number of beads) where compared in the current study.

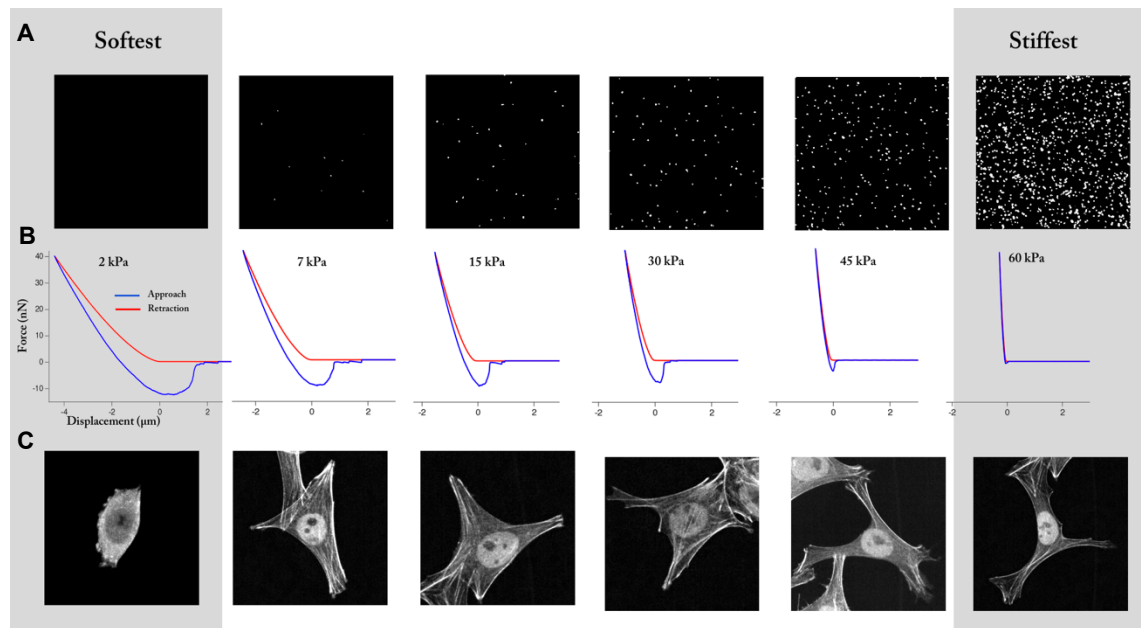


Figure 20. HeLa H2B-cells imaged at different location of the hydrogel gradient. Grey highlight shows both extremes of the gradient, no beads (softest region of the hydrogel) and high density of beads (stiffest region of the hydrogel). **A)** Gradient of beads. **B)** Example of force curves that correspond to the stiffness inferred from the density of beads. **C)** HeLa H2B-GFP cell phenotype across the hydrogel gradient of stiffness. Phenotypic changes occur already where a few beads are present (~ 7 KPa) and this phenotype is maintained across the rest of the gradient.

The appropriate microscope laser lines and filter sets were chosen to image the intracellular distribution of mechanoresponsive proteins (YAP/TAZ, Oct-1 and MASTL), cell actin and cell nucleus. A Z-stack ($324.48 \mu\text{m} \times 324.48 \mu\text{m} \times 14 \mu\text{m}$) was acquired for each location containing various cells. The beads at the same location were acquired by changing the focal plane to the most upper layer of the hydrogel (underneath the cell) and this plane was used as a z-top limit for the Z-stack ($324.48 \mu\text{m} \times 324.48 \mu\text{m} \times 7 \mu\text{m}$).

Image processing and analysis

Nuclear to cytoplasmic ratio of mechanoresponsive proteins (YAP/TAZ, Oct1 and MASTL): A semi-automatic custom macro script (ImageJ, Fiji) was used to analyse cell nuclear to cytoplasmic intensity ratio of YAP/TAZ, Oct-1 or MATL. Briefly, the macro performed the following steps:

1. Maximum intensity projection of stacks from mechanoresponsive proteins (YAP/TAZ, Oct1 or MATL) and cell nucleus.
2. Segmentation of the cell nucleus and $1 \mu\text{m}$ cytoplasm segmentation around the cell nucleus.

3. Generation of an .xlsx file containing, for each cell in the image, the mean intensity value of the corresponding protein at the cell nucleus and at the segmented cytoplasmic region.

The intensity ratio for each cell was then calculated dividing the mean intensity in the nucleus by the mean intensity in the cytoplasm (*Figure 21*). A value of 1 indicates no difference of protein levels between both cellular compartments, a ratio higher than 1 indicates higher presence of the protein in the nuclear compartment and a ratio lower than 1 indicates higher presence of the protein in the cytoplasm.

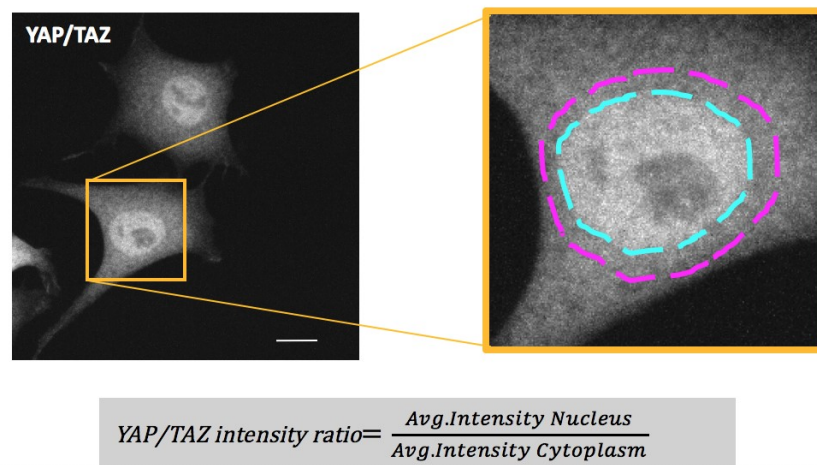
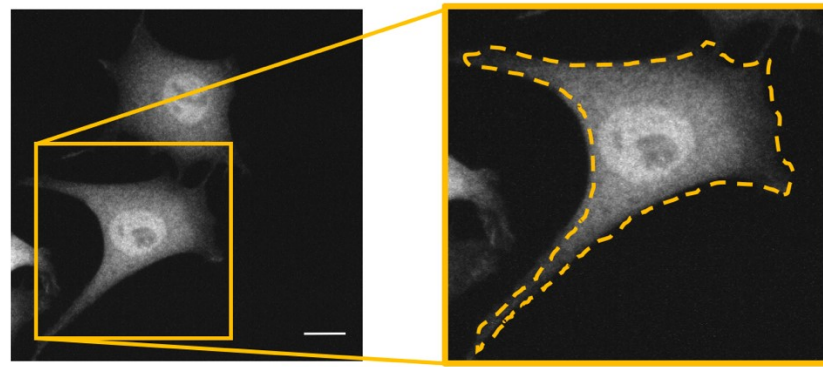


Figure 21. YAP/TAZ nuclear to cytoplasmic intensity ratio. HeLa H2B-GFP cell stained for YAP/TAZ. Scale bar, 10 µm. Close-up view of YAP/TAZ intracellular expression showing the cell nucleus segmentation (blue line) and 1 µm cytoplasmic segmentation around the nucleus performed by the macro described in this section.

Cell area (µm²) and circularity (a.u.): A semi-automatic custom macro script (ImageJ, Fiji) was used to measure cell area (µm²) and circularity (a.u.). Briefly, the macro performed the following steps:

1. Maximum intensity projection of stacks from the channel containing the mechanoresponsive proteins (YAP/TAZ, Oct1 or MATL).
2. Segmentation of the whole cell, including nucleus and total cytoplasm.
3. Generation of an .xlsx file containing, for each cell in the image, the cell total area (µm²) and the cell circularity (a.u.).

The circularity of the cell is calculated by the operation $4\pi \cdot \text{area} / (\text{perimeter})^2$, where a value of 1 indicates a perfect circle (*Figure 22*). As the value approaches 0, it indicates an increasingly elongated shape.



$$\text{circularity (a.u)} = \frac{4\pi \cdot \text{area}}{(\text{Perimeter})^2}$$

Figure 22. HeLa H2B cell stained for YAP/TAZ. Scale bar, 10 μm (Left). Close up view of the cell segmented area and formula for the circularity (Right).

Assessment of FAs number and size: Quantity and size of cell FAs were assessed by visual inspection. Different available macros for object segmentation were tested in order to perform a quantitative analysis of cell FAs. However, FAs are complex structures and were difficult to identify by any of the available automatic macros without selecting noise or other structures that were not FAs. For this reason and, because the visual inspection allowed to easily see the differences in number and size of FAs between the stiff and soft regions of the gel, it was decided to simply assess them visually.

Quantification of beads: At each gel location where cells were acquired, a different channel was used to obtain the beads. The semi-automatic macro script (Fiji) was used to segment and quantify the beads. Each stack of images was processed individually in order to select the most appropriate threshold value for an accurate segmentation of the beads. Then, the density of beads per area ($1/10^4 \mu\text{m}^2$) was calculated for each image as described in section 3.2.3.

Only cells located at those parts of the hydrogel corresponding to the softest region (< 2.5 KPa) and stiffest region (> 50 KPa), were used in the statistical analysis.

Statistical analysis

Three independent hydrogels ($n=3$) and approximately 70-80 cells at each stiffness extreme of the gradient, stiffest part (>50 KPa) and softest (<2.5 KPa), were used in the statistical analysis. To analyse statistical differences between cells on the stiff and the soft region of the gel, three independent t-tests for each mechanoresponsive protein (YAP/TAZ, MASTL and Oct1) and for each gel were carried out. One t-test to study differences in nuclear to cytoplasmic protein intensity, one for cell area and one for cell

roundness. In total, 27 independent t-tests (3 proteins x 3 gels x 3 parameters under study) were carried out.

4. RESULTS

4.1. Fabrication of PA bead-containing stiffness gradient hydrogels

Two protocols for the fabrication of gradient hydrogels were developed, one to fabricate hydrogels with a stiffness gradient ranging from ~ 2 KPa to 60 KPa (wide-range hydrogel) and another to fabricate hydrogels with a stiffness gradient ranging from ~ 0.5 KPa to 22 KPa (narrow-range hydrogel). Both protocols included a step where fluorescent beads were incorporated in the PA mixture expecting to obtain a gradient of beads that correlates with the stiffness gradient. The main difference between the two types of hydrogels was the PA premixes used to generate the desired stiffness range. Additionally, the protocol of the narrow-range hydrogel introduced the use of a petri dish with a gridded glass-bottom. The new mould aimed to improve the generation of the correlation curve between beads and stiffness during next steps of the methodology. See protocols' description in section 3.1 for details.

The results presented in this section provides a list of aspects that need to be considered for the fabrication and usability of the hydrogels.

Characteristics of the fabrication protocols:

- Basic material and reagents required: glass-bottom petri dishes, circular coverslips, Bind-silane, PA solutions, PBS, FluoSpheres, APS and TEMED solutions.
- Fabrication time: ~ 2 h 30min to 3h.
- Reproducibility: From two PA solutions (~ 450 μ l to 500 μ l), one soft and one stiff, 5 gradient hydrogels can be fabricated in one batch. After the fabrication of 30 batches, the qualitative estimation provides a success rate of 4 out of 5 hydrogels.

Properties of the gradient hydrogels

- Shape: round.
- Diameter: 14 mm.
- Thickness: $\sim 80 \pm 100$ μ m.
- Surface: slightly tilted and small wrinkles around the gel edges.
- Colour: translucent and gradual fluorescent green under fluorescence microscope.
- Bead gradient area: ~ 6 mm (W) x 2 mm (H).

The generated hydrogels show a distribution of beads with three differentiated regions (*Figure 23***Figure 1**): a region without beads or very low quantity of beads

that covers a small area located in the upper half of the gel; a region with a gradient of beads contained within an area of approximately 6 mm (W) x 2 mm (H), located in the middle-upper part of the gel; and a region with the maximum number of beads that covers a big area, approximately from the middle to the bottom part of the gel.

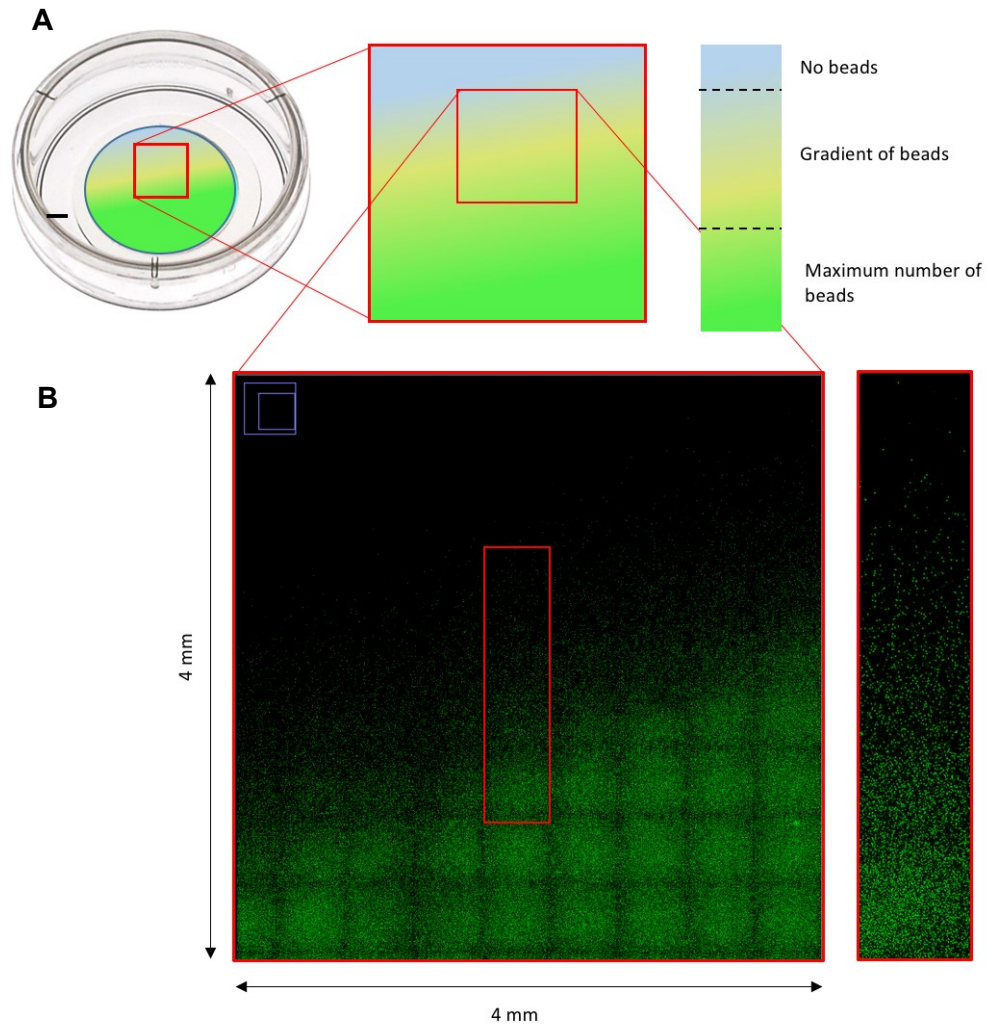


Figure 23. Distribution of fluorescent beads within the gradient hydrogels. **A)** General illustration of how beads are distributed within the gel and close-up view of the three distinguished regions: blue, no beads; yellow, gradient of beads; and green, maximum number of beads. **B)** Real tile scan example of the 4 mm x 4 mm region acquired for the beads and close-up view of the gradient.

4.2. Generation of the correlation curves between fluorescent beads and stiffness

Three hydrogels of each type, wide range (~ 2 KPa to 60 KPa) and narrow range (~ 0.5 KPa to 22 KPa), were fabricated. For each hydrogel: (1) the beads were acquired (by SDCM) and quantified, and the stiffness was characterized (by AFM). Detail description of the procedure can be found in section 3.2.

The data from the three independent hydrogels (n=3) was combined for each hydrogel type. Next, Igor Pro software was used to plot the bead density against the stiffness and to calculate the best fitting curve to the data.

The results presented in the following sections show: (1) an example of the data obtained from one hydrogel of each type and (2) two correlation curves that best fit the data for three combined hydrogels of each type.

4.2.1. Wide-range gradient hydrogel: ~2 KPa to 60 KPa

Figure 24 and Figure 25 show an example of the data obtained from one, out of the three, wide-range hydrogels:

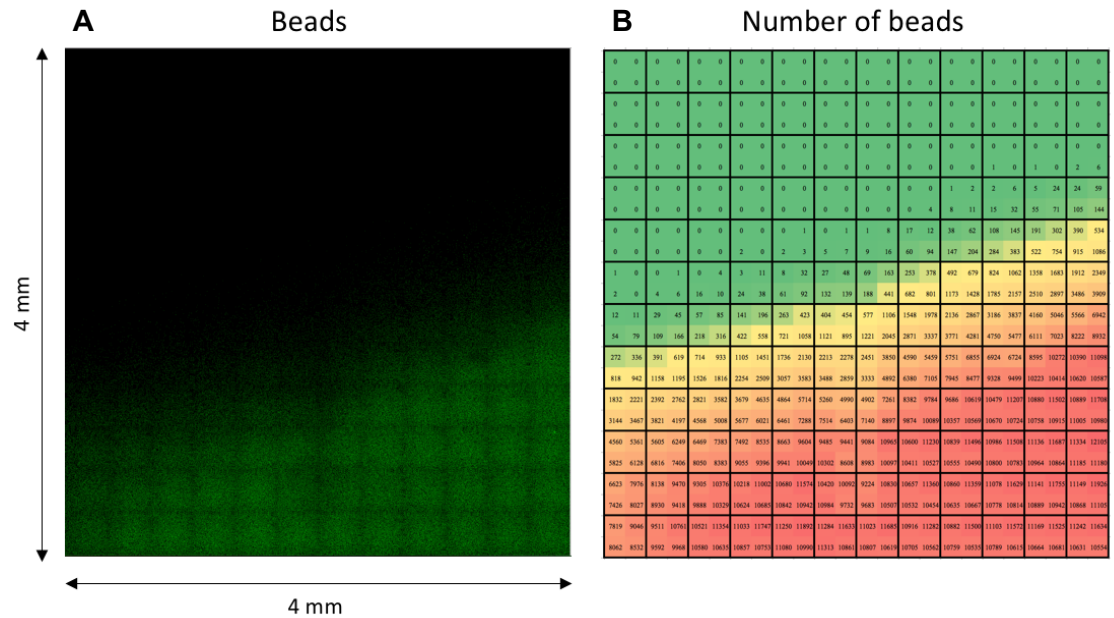


Figure 24. A) Tile scan montage of the acquired beads covering a 4 mm x 4 mm area of the hydrogel. B) 2D matrix containing the number of beads spatial distribution (4 values per image).

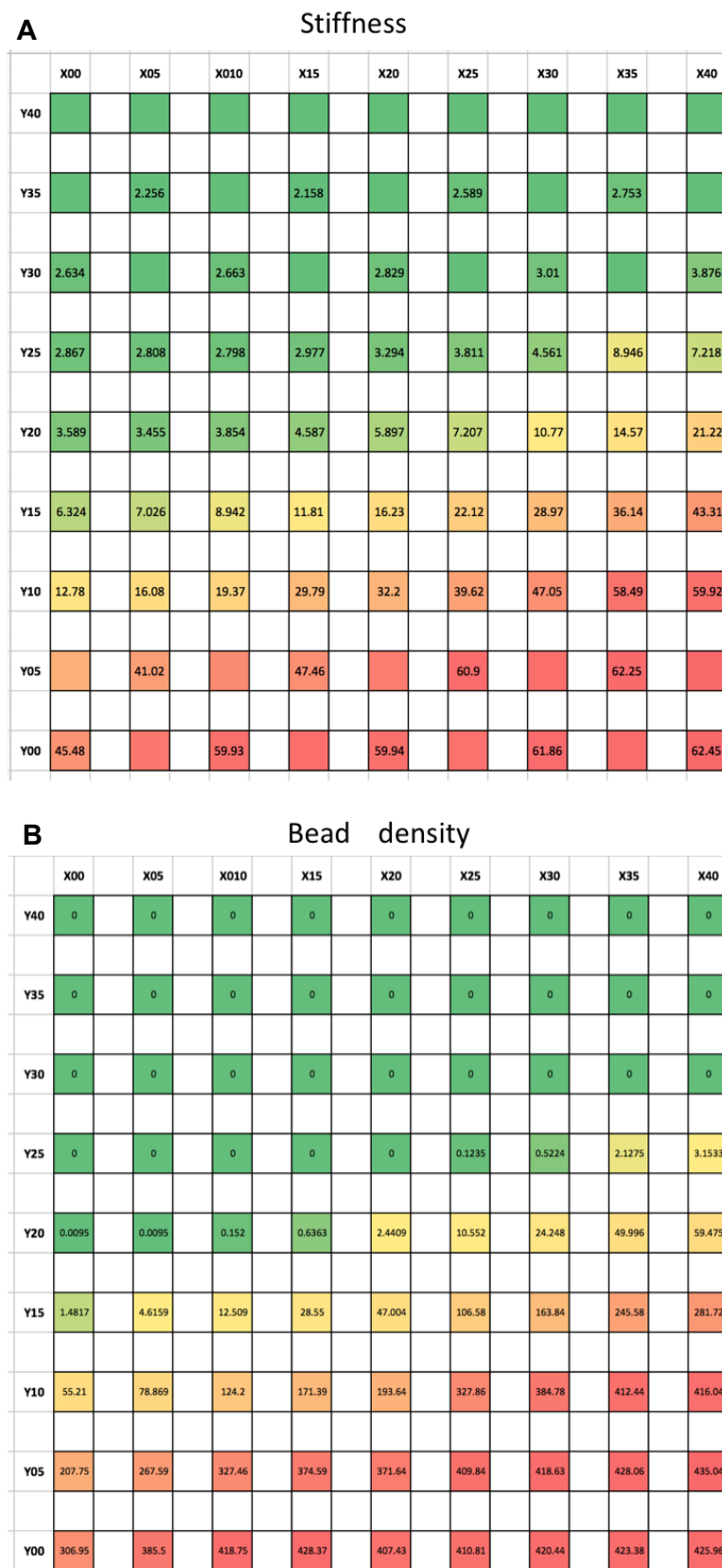


Figure 25. **A)** 2D matrix containing the averaged stiffness. Missing values correspond to those locations where the stiffness was not measured. **B)** 2D matrix containing the averaged bead density per area ($1/10^4 \mu\text{m}^2$) calculated from data in *Figure 24*. Only those locations where stiffness was measured were used to generate the correlation curve.

The density of beads per area and stiffness from three independent hydrogels (~2 KPa to 60 KPa) was measured and calculated as described in section 3.2. All data were then combined in order to generate the final correlation curve. Igor Pro Software was used to plot bead density against stiffness and to calculate the best fitting curve to the data (*Figure 26*). The correlation curve exhibits a linear relationship at intermediate bead density/stiffness values while displaying significant changes in stiffness with very little change in bead density at both extremes. Bead density shows to be saturated at approximately 60 KPa of stiffness and the bead density SE exhibits higher values at intermediate locations.

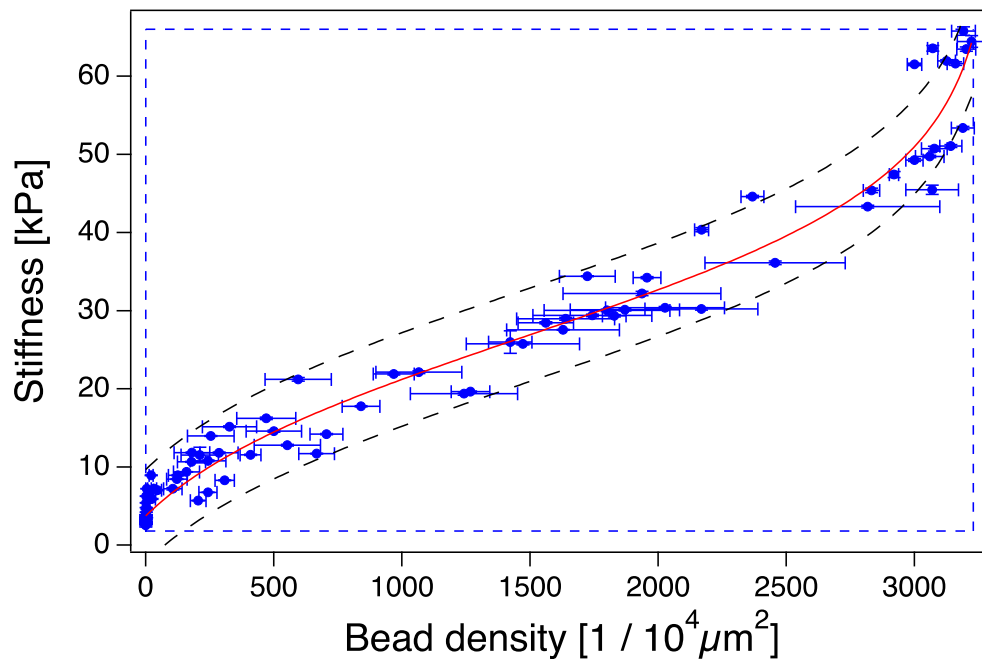


Figure 26. Wide-range correlation curve (~2 KPa to 60 KPa) between bead density and stiffness (Igor Pro Software). Each data point shows the SE for the averaged bead density (horizontal error bar; averaged of the four closest values) and the SE for the averaged stiffness (vertical error bar; nine indentation points at each location). Black discontinuous line at both sides of the curve corresponds to the interval of confidence (IC)

The generic equation of the best model describing this behaviour corresponds to a so-called Logit function (*Equation 2*).

$$y(x) = y_{half} - \left\{ rate * \left(\log \left(\left(\frac{max}{(x - min)} \right) - 1 \right) \right) \right\}$$

Equation 2. Logit function

Equation 3 is the same Logit formula with the values (invariable coefficients \pm one standard deviation) returned by Igor Pro based on the data. Where x corresponds to the density of beads per area at a certain location. By inputting x , the equation returns the corresponding stiffness at that location.

$$y(x) = 26.704 \mp 0.805 - \left\{ 23.631 \mp 1.74 * \left(\log \left(\left(\frac{3668.9 \mp 113}{(x - 354.09 \mp 83.2)} \right) - 1 \right) \right) \right\}$$

Equation 3. Logit function with corresponding values

4.2.2. Narrow-range correlation curve: stiffness range from ~ 0.5 KPa to 22 KPa

Figure 27 and *Figure 28* show an example of the data obtained from one, out of the three, narrow-range hydrogels:

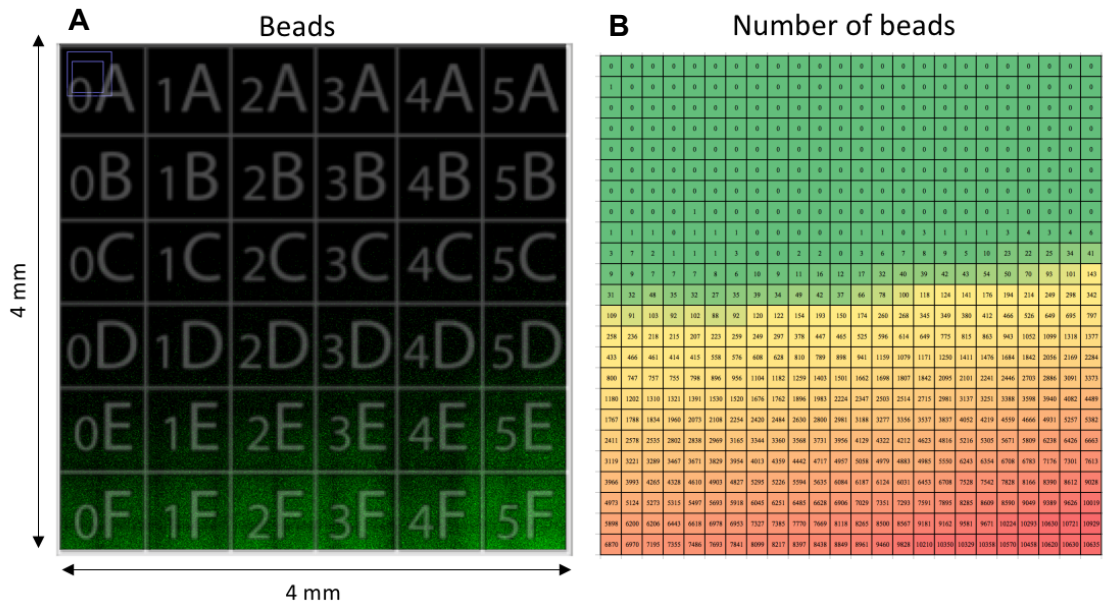


Figure 27. A) Overlapped tile scan montage of the beads and the gridded glass bottom of the petri dish (4 mm x 4 mm area of the hydrogel). B) 2D matrix containing the number of beads spatial distribution (4 values per image).

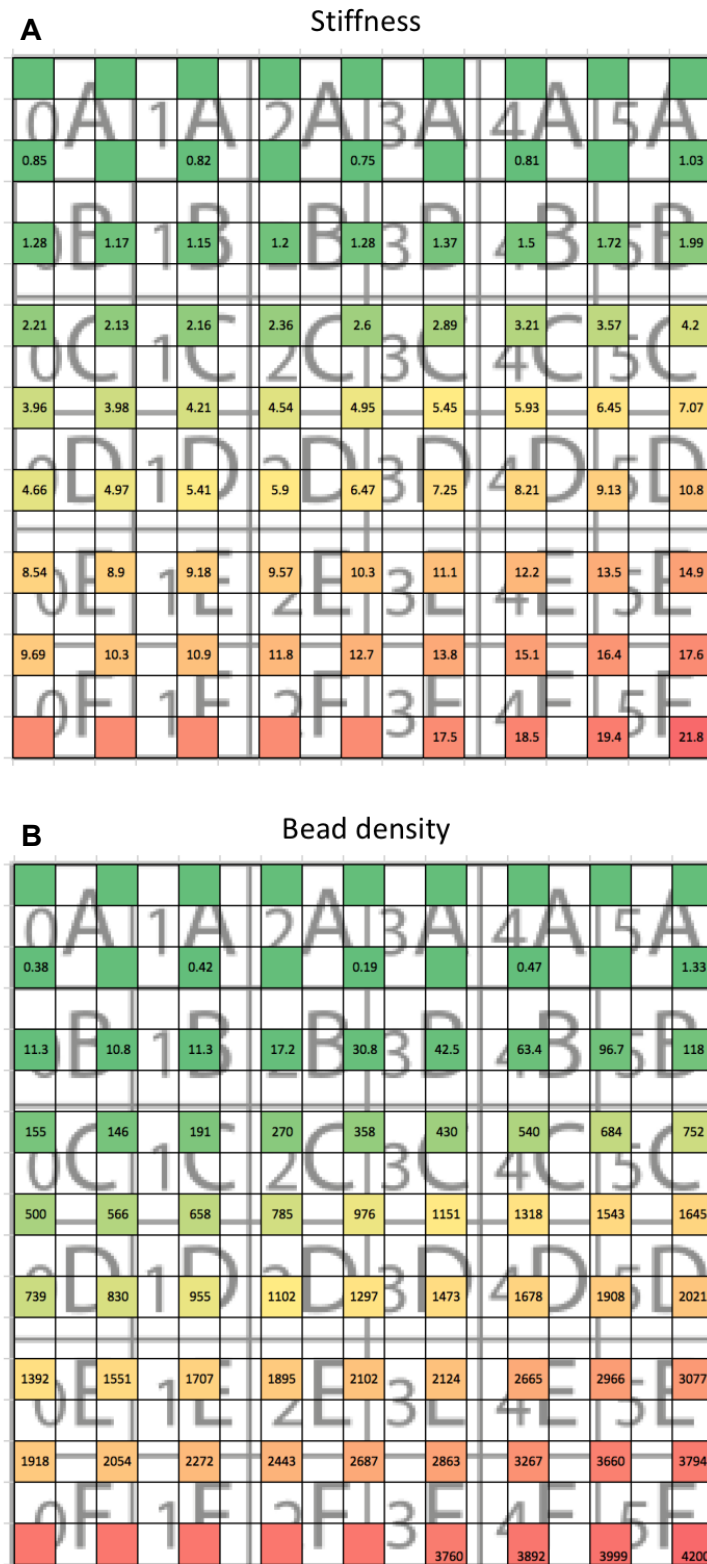


Figure 28. **A)** 2D matrix containing the averaged stiffness spatial distribution and gridded glass-bottom of the petri dish. Missing values correspond to those locations where the stiffness was not measured. **B)** 2D matrix containing the averaged bead density per area ($1/10^4 \mu\text{m}^2$), calculated from data in *Figure 27*, and overlapped montage of the gridded glass-bottom. Only those locations where stiffness was measured were used to generate the correlation curve.

The density of beads per area and stiffness from three independent hydrogels (~ 0.5 KPa to 22 KPa) was measured and calculated as described in section 3.2. All data was then combined in order to generate the final narrow-range correlation curve. Igor Pro Software was used to plot bead density ($1/10^4 \mu\text{m}^2$) against stiffness (KPa) and to calculate the best fitting curve to the data (*Figure 29*). The correlation curve exhibits a linear relationship ($R^2 = 0.966$) with maximum stiffness values of approximately 22 KPa.

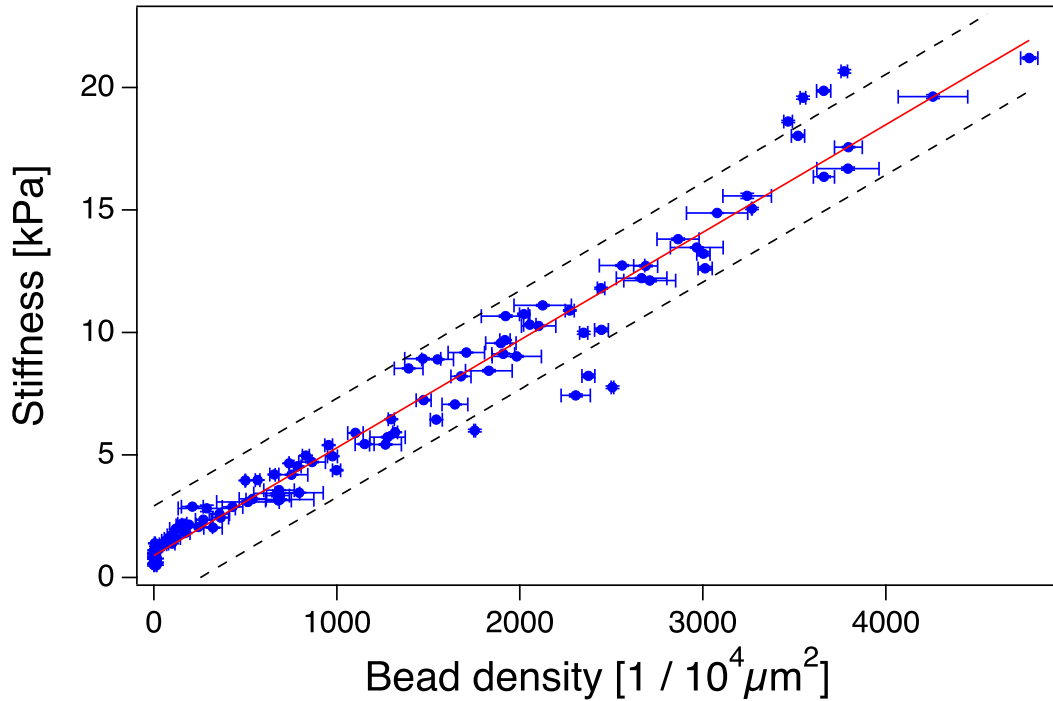


Figure 29. Narrow-range correlation curve (~ 0.5 KPa to 22 KPa) between bead density and stiffness (Igor Pro Software). Each data point shows the SE for the averaged bead density (horizontal error bar; averaged of the four closest values) and the SE for the averaged stiffness (vertical error bar; nine indentations points at each location). Black discontinuous line at both sides of the curve corresponds to the IC.

The generic equation of the best model describing this behaviour corresponds to a linear function (*Equation 4*).

$$y = a * x + b$$

Equation 4. Linear function

Equation 5 is the same linear function with the values (invariable coefficients \pm one standard deviation) returned by Igor Pro based on the data. Where x corresponds to the density of beads per area at a certain location. By inputting x , the equation returns the corresponding stiffness at that location.

$$y = 0.0044 * x + 0.903$$

Equation 5. Linear function with corresponding values

4.3. Validation of the wide-range (2 KPa to 60 KPa) correlation curve

The validation of the wide-range hydrogel was carried out from two perspectives:

(1) Quantitative validation, which aimed to quantify the error of *Equation 3* with respect to the ground truth. (section 3.3.1)

(2) Biological validation, which aimed to test the usability of the hydrogels for cell culture studies. For this, HeLa H2B-GFP cells were cultured on the gradient hydrogels and different aspects regarding cellular mechano-responsiveness to substrate stiffness were studied (section 3.3.2)

4.3.1. Quantitative validation

Figure 30 and *Figure 31* show the results of the hydrogel used for the quantitative validation.

Bead density

0	0	0	0	0.08	0	0	0	0
0	0	0	0	0	0	0	0	0
0.23	0.08	0	0.08	0.08	0.15	0.31	0.62	1.31
40.9	36.7	34.9	38.8	34.7	45.7	50.4	53.3	59.8
385	366	389	418	474	644	843	1224	1342
1520	1557	1743	2032	2327	2691	2943	3233	3239
3954	3871	3947	3822	3862	3799	3695	3576	3533
3870	3893	3862	3833	3802	3712	3574	3425	3376
3916	3855	3884	3849	3767	3686	3501	3364	3300

Figure 30. 2D matrix with the spatial distribution of the averaged bead density.

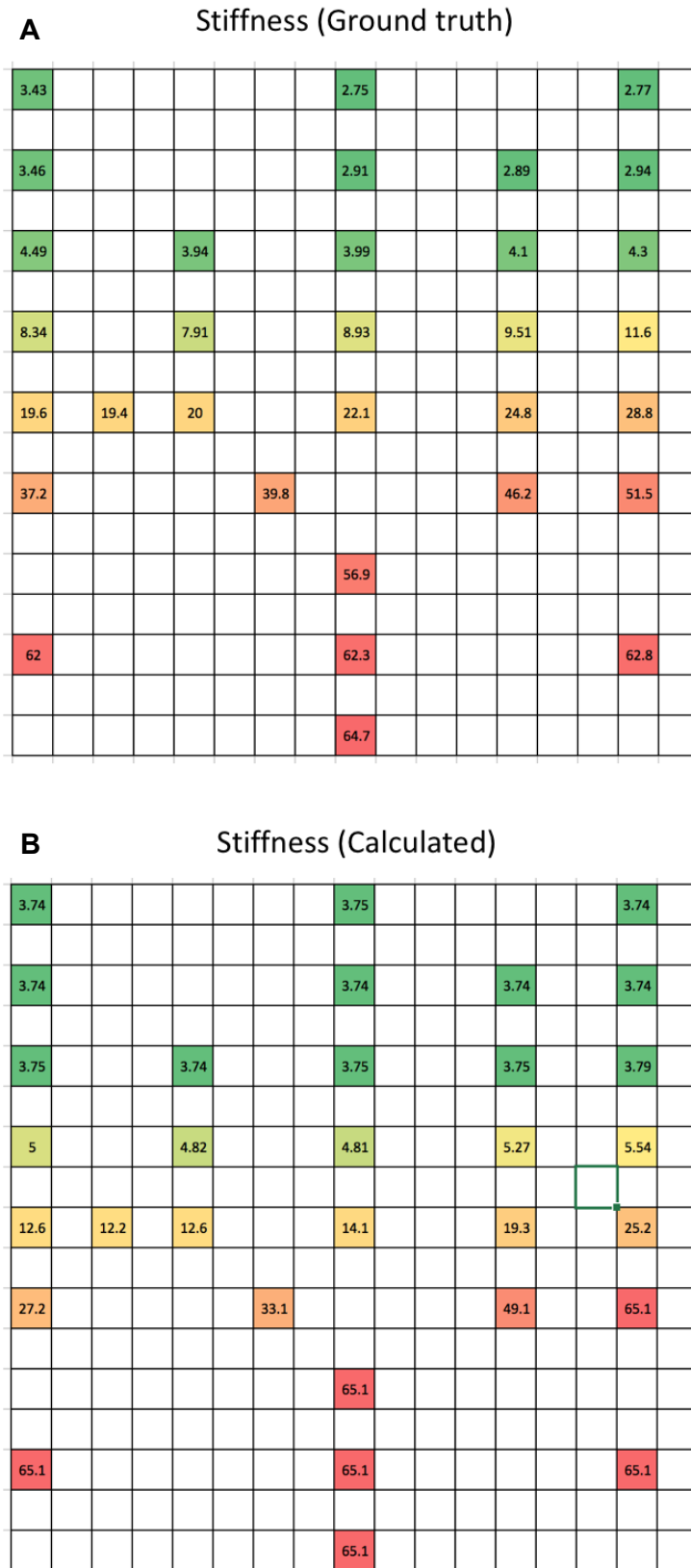


Figure 31. **A)** Real stiffness (ground truth) measured at random locations with the AFM within the hydrogel ROI **B)** Calculated stiffness at same locations by inputting the known x value (density of beads per area) in *Equation 3*.

The averaged SE between the ground truth stiffness and the calculated stiffness is approximately of 3 KPa within a range of 0.19 KPa to 14 KPa.

Plotting the ground truth stiffness against the calculated bead density and comparing it with the wide-range correlation curve shows that the data is within the IC of the curve (*Figure 32*).

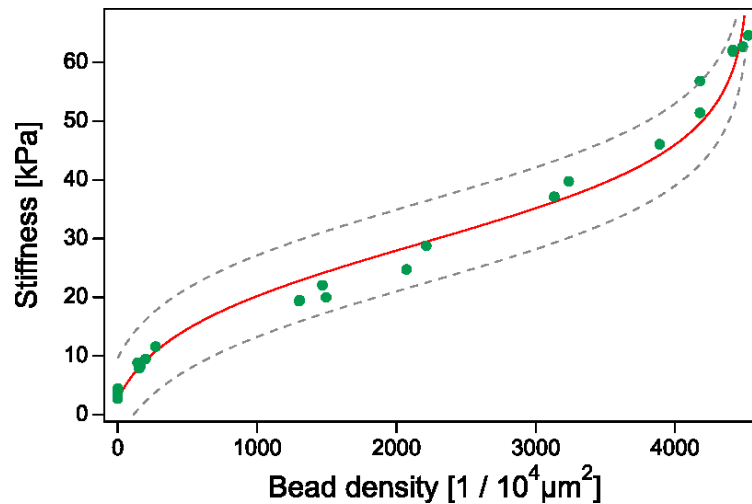


Figure 32. Wide-range correlation curve (red line) with its calculated IC (dotted lines) and plotted data of ground truth stiffness against calculated bead density (green dots).

4.3.2. *Biological validation*

HeLa H2B-GFP cells were cultured on wide-range hydrogels. Cells located on both extremes of the gradient, softest region/no beads (< 2.5 KPa) and stiffest region/high density of beads (>50 KPa), were compared. Three aspects of cell mechanoresponsiveness to substrate stiffness were studied (see section 3.3.2).

(1) Nuclear to cytoplasmic ratio of mechanoresponsive proteins: YAP/TAZ, Oct1 and MASTL

Figure 33 shows example images of cells located on the stiff region of the hydrogel (>50 KPa) and cells located on the softer region (<2.5 KPa). Cells located on the stiff region express higher nuclear intensity of YAP/TAZ, Oct1 and MASTL while cells located on the soft region express lower nuclear intensity.

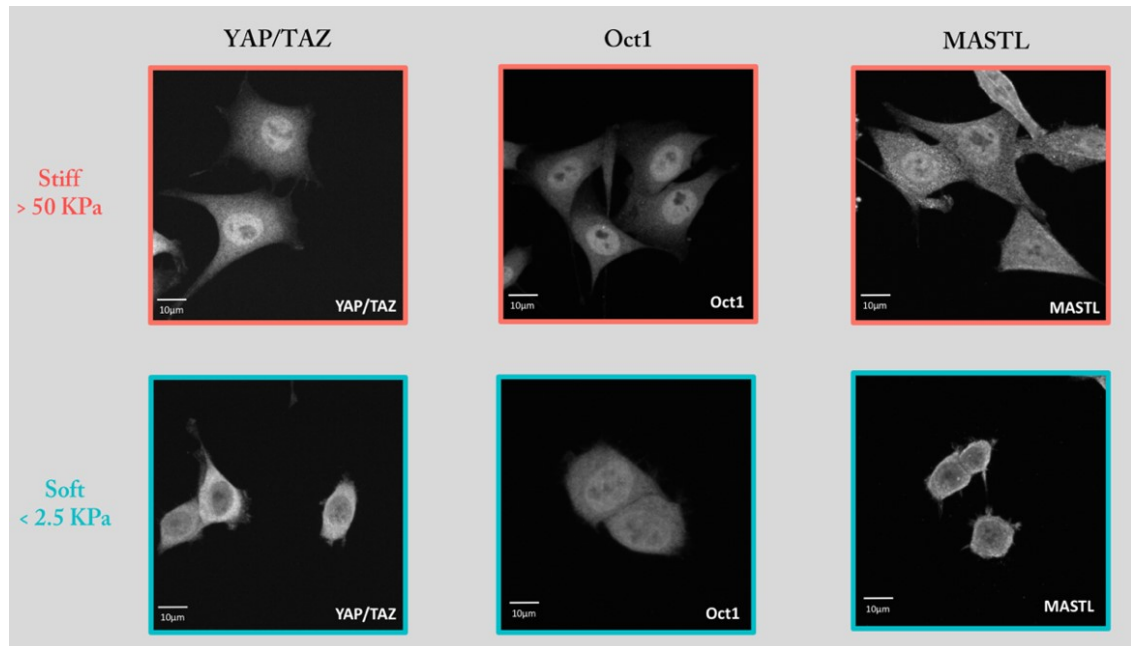


Figure 33. HeLa H2B-GFP cells cultured on wide-range gradient hydrogels. From left to right, cells stained for the three mechanoresponsive proteins: YAP/TAZ, Oct1 and MASTL. First row images correspond to cells located at stiffest region of the hydrogel (> 50 KPa) and second row images correspond to cells located at softest region of the hydrogel (< 2.5 KPa).

Figure 34 shows the boxplots with the quantitative analyses of intensity ratio for YAP/TAZ. Cells from three independent hydrogels were analysed and statistically compared. Nuclear to cytoplasmic intensity ratio of YAP/TAZ was significantly higher ($p < 0.001$) in cells that were located on the stiffest regions of the hydrogel compared with those located on the softest regions (Table 2).

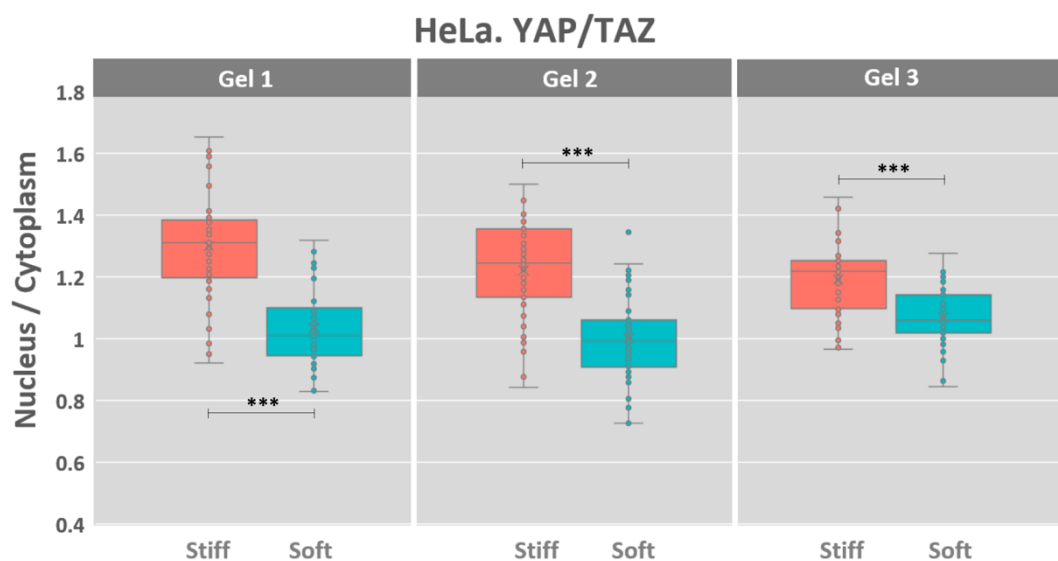


Figure 34. Boxplots of YAP/TAZ nuclear to cytoplasmic intensity ratio. Gel 1,2,3 correspond to three independent samples (different hydrogels and seeding days). Orange boxplots show the data

of cells located on stiffest regions (> 50 KPa) and blue boxplots show the data of cells located on softest region (< 2.5 KPa) ($n=70$ to 80 cells; $***$ p -value < 0.001).

Figure 35 shows the boxplots with the quantitative analyses of intensity ratio for Oct1. Cells from three independent hydrogels were analysed and statistically compared. Nuclear to cytoplasmic intensity ratio of Oct1 was significantly higher ($p < 0.001$) in cells located on the stiffest regions of the hydrogel compared with those located on the softest regions (Table 2).

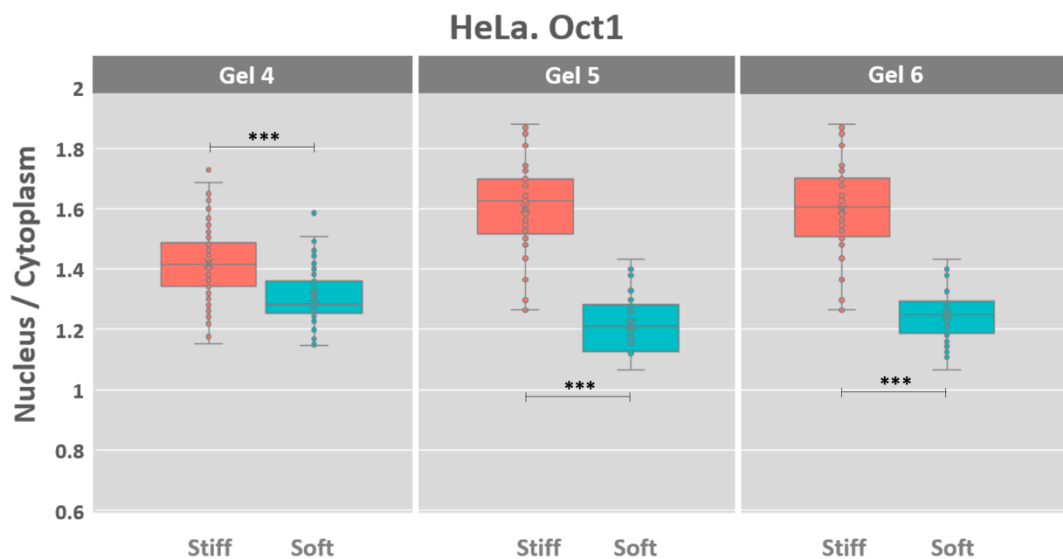


Figure 35. Boxplots of Oct1 nuclear to cytoplasmic intensity ratio. Gel 4,5,6 correspond to three independent samples (different hydrogels and seeding days). Orange boxplots show the data of cells located on stiffest regions and blue boxplots show the data of cells located on softest region. ($n=70$ to 80 cells; $***$ p -value < 0.001).

Figure 36 shows the boxplots with the quantitative analyses of intensity ratio for MASTL. Cells from three independent hydrogels were analysed and statistically compared. Nuclear to cytoplasmic intensity ratio of MASTL resulted to be significantly higher ($p < 0.001$) in cells that are located on the stiffest regions of the hydrogel compared with those located on the softest regions (Table 2).

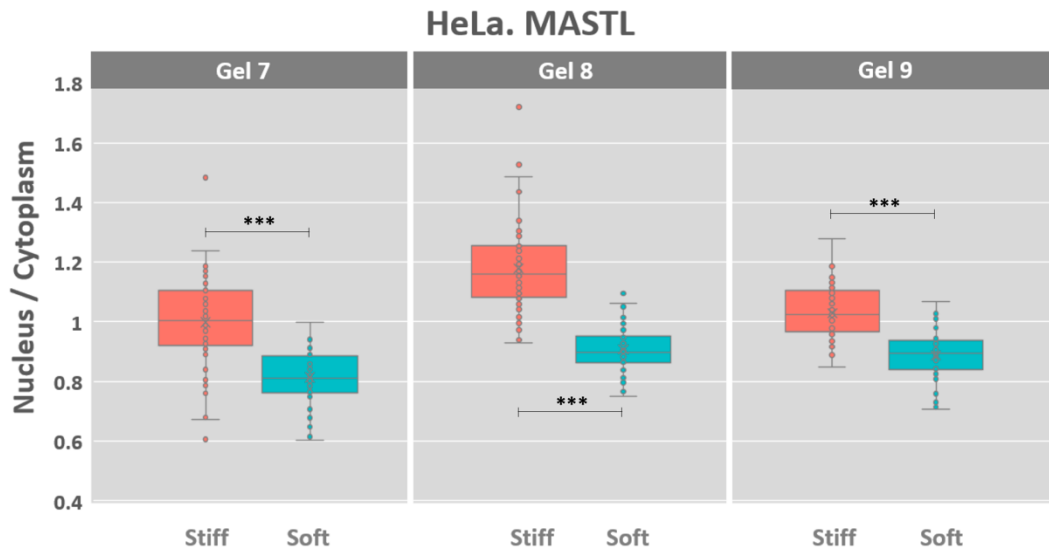


Figure 36. Boxplots of MASTL nuclear to cytoplasmic intensity ratio. Gel 7,8,9 correspond to three independent samples (different hydrogels and seeding days). Orange boxplots show the data of cells located on stiffest regions and blue boxplots show the data of cells located on softest region. (n=70 to 80 cells; *** p-value < 0.001)

(2) Cell area (μm^2) and circularity (a.u.)

In *Figure 33* it can be observed that cells located on the stiff region of the gradient (> 50 KPa) seem to have higher area (μm^2) and lower circularity than those falling on the soft region of the gradient (< 2.5 KPa).

The same cells that were analysed in the previous section, were also analysed to determine cell area and circularity. *Figure 37*, *Figure 38* and *Figure 39* show the boxplots of both measurements, cell area and circularity, corresponding to cells stained for YAP/TAZ, Oct1 and MASTL. In the three cases, cell area was significantly higher in cells located on the stiffest regions while cell circularity was inversely proportional at those regions (Table 2).

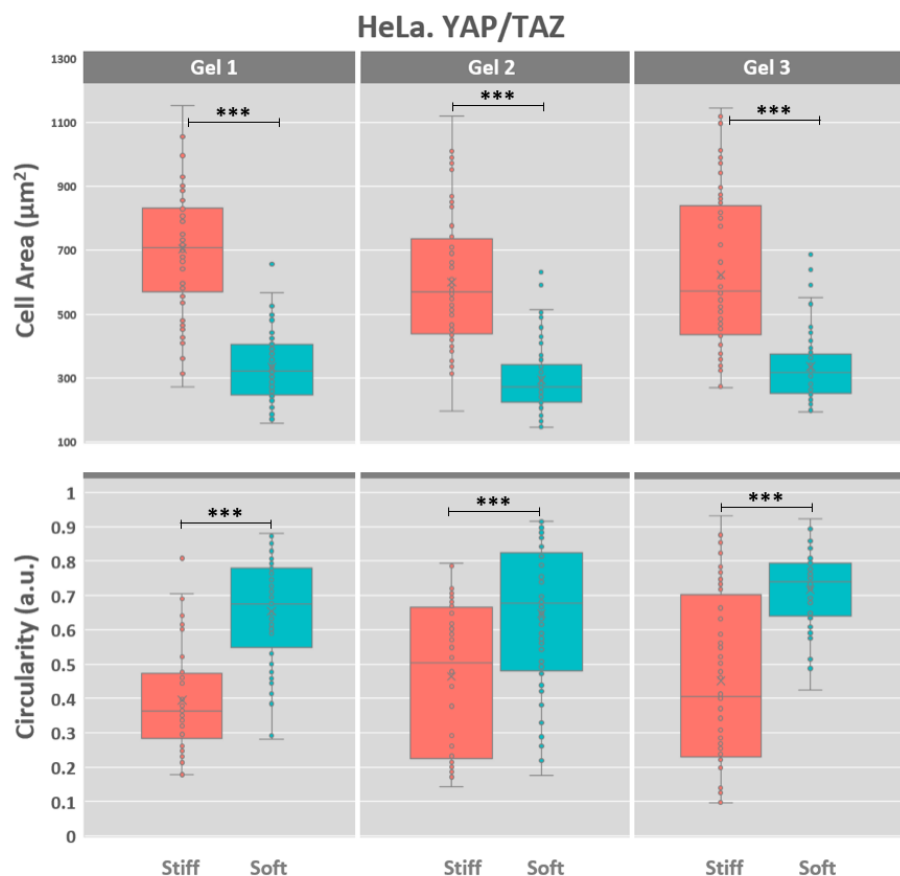


Figure 37. Hydrogels 1,2,3 correspond to the three independent samples used in YAP/TAZ ratio analysis. In first row, boxplots with HeLa cell area (μm^2). In second row, boxplots with HeLa circularity (a.u.). Orange boxplots show the data of cells located on the stiffest regions (>50 KPa) and blue boxplots show the data of cells located on the softest region (<2.5 KPa) ($n=70$ to 80 cells; *** p-value < 0.001)

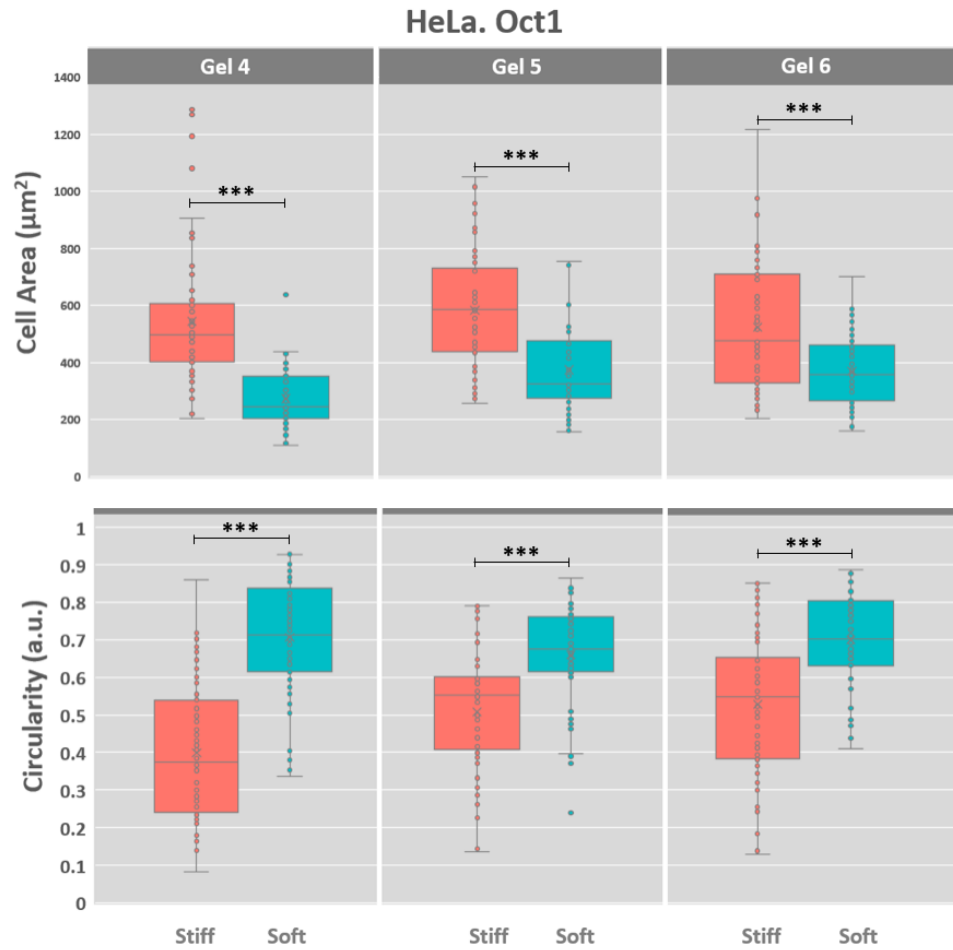


Figure 38. Hydrogels 4,5,6 correspond to the three independent samples used in Oct1 ratio analysis. In first row, boxplots with HeLa cell area (μm^2). In second row, boxplots with HeLa circularity (a.u.). Orange boxplots show the data of cells located on the stiffest regions (>50 KPa) and blue boxplots show the data of cells located on the softest region (<2.5 KPa; $n=70$ to 80 cells; *** p-value < 0.001).

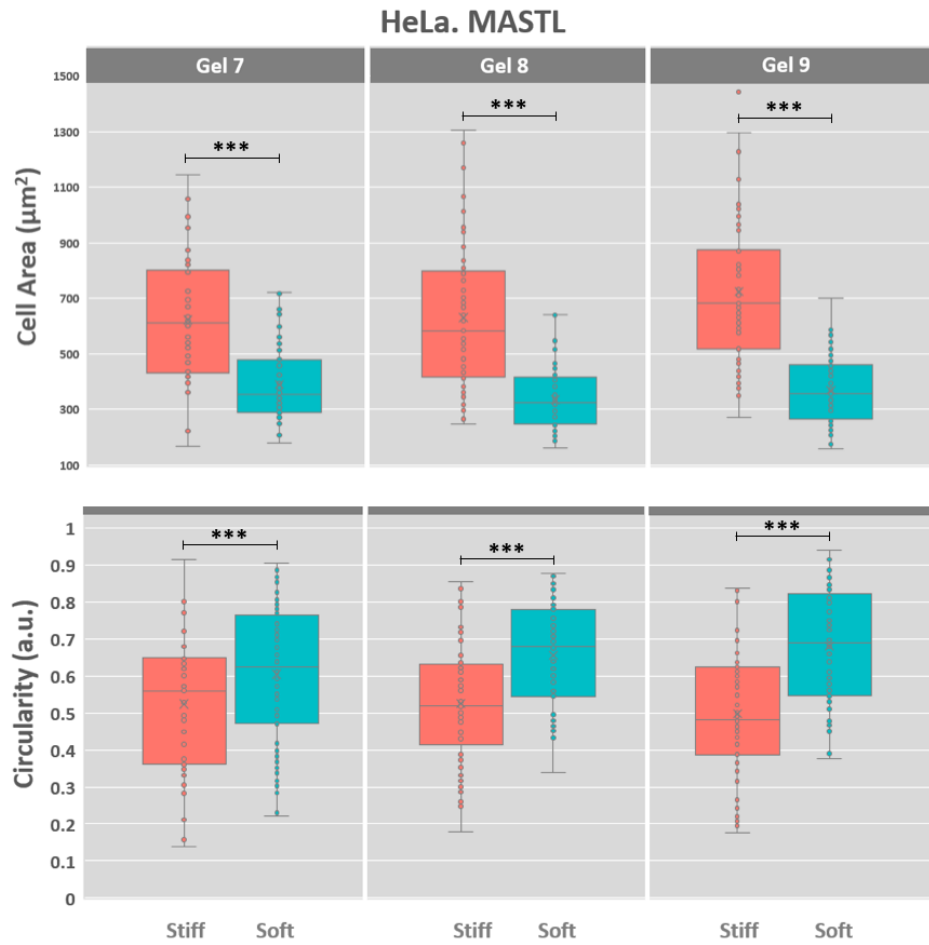


Figure 39. Hydrogels 7,8,9 correspond to the three independent samples used in MASTL ratio analysis. In first row, boxplots with HeLa cell area (μm^2). In second row, boxplots with HeLa circularity (a.u.). Orange boxplots show the data of cells located on the stiffest regions (>50 KPa) and blue boxplots show the data of cells located on the softest region (<2.5 KPa: $n=70$ to 80 cells; *** p-value < 0.001).

Table 2. Statistical results of the biological validation for wide-range gradient hydrogels.

		Intensity Ratio (nuclear/cytoplasmic)		Area (μm^2)		Circularity (a.u.)	
		M (SD)	p-value	M (SD)	p-value	M (SD)	p-value
YAP/TAZ	Gel 1 Stiff	1.30 (0.17)	p<0.001	705.50 (210.17)	p<0.001	0.39 (0.14)	p<0.001
	Gel 1 Soft	1.03 (0.13)		333.54 (106.86)		0.65 (0.15)	
	Gel 2 Stiff	1.22 (0.15)	p<0.001	600.61 (211.30)	p<0.001	0.46 (0.22)	p<0.001
	Gel 2 Soft	1.00 (0.13)		293.20 (106.75)		0.65 (0.21)	
	Gel 3 Stiff	1.19 (0.11)	p<0.001	622.54 (242.92)	p<0.001	0.45 (0.26)	p<0.001
	Gel 3 Soft	1.07 (0.09)		335.71 (113.15)		0.72 (0.12)	
Oct1	Gel 4 Stiff	1.42 (0.12)	p<0.001	544.65 (234.67)	p<0.001	0.40 (0.18)	p<0.001
	Gel 4 Soft	1.31 (0.09)		273.52 (99.31)		0.71 (0.15)	
	Gel 5 Stiff	1.6 (0.16)	p<0.001	582.66 (203.58)	p<0.001	0.51 (0.15)	p<0.001
	Gel 5 Soft	1.22 (0.09)		374.07 (141.12)		0.66 (0.13)	
	Gel 6 Stiff	1.6 (0.17)	p<0.001	524.47 (221.34)	p<0.001	0.53 (0.18)	p<0.001
	Gel 6 Soft	1.25 (0.08)		319.76 (87.77)		0.70 (0.12)	
MASTL	Gel 7 Stiff	1.00 (0.16)	p<0.001	622.33 (218.28)	p<0.001	0.52 (0.17)	p<0.001
	Gel 7 Soft	0.81 (0.09)		389.44 (134.88)		0.60 (0.19)	
	Gel 8 Stiff	1.18 (0.14)	p<0.001	631.90 (252.63)	p<0.001	0.52 (0.16)	p<0.001
	Gel 8 Soft	0.91 (0.08)		334.94 (113.12)		0.65 (0.14)	
	Gel 9 Stiff	1.03 (0.09)	p<0.001	724.47 (263.02)	p<0.001	0.50 (0.17)	p<0.001
	Gel 9 Soft	0.89 (0.08)		369.64 (120.73)		0.68 (0.15)	

(3) Assessment of FA number and size

Figure 40 shows example images demonstrating visually that the number and size of cell FA is higher in cells located on the stiff region of the hydrogel while cells located on the soft region of the hydrogel form very few and small FA, or none, of these structures.

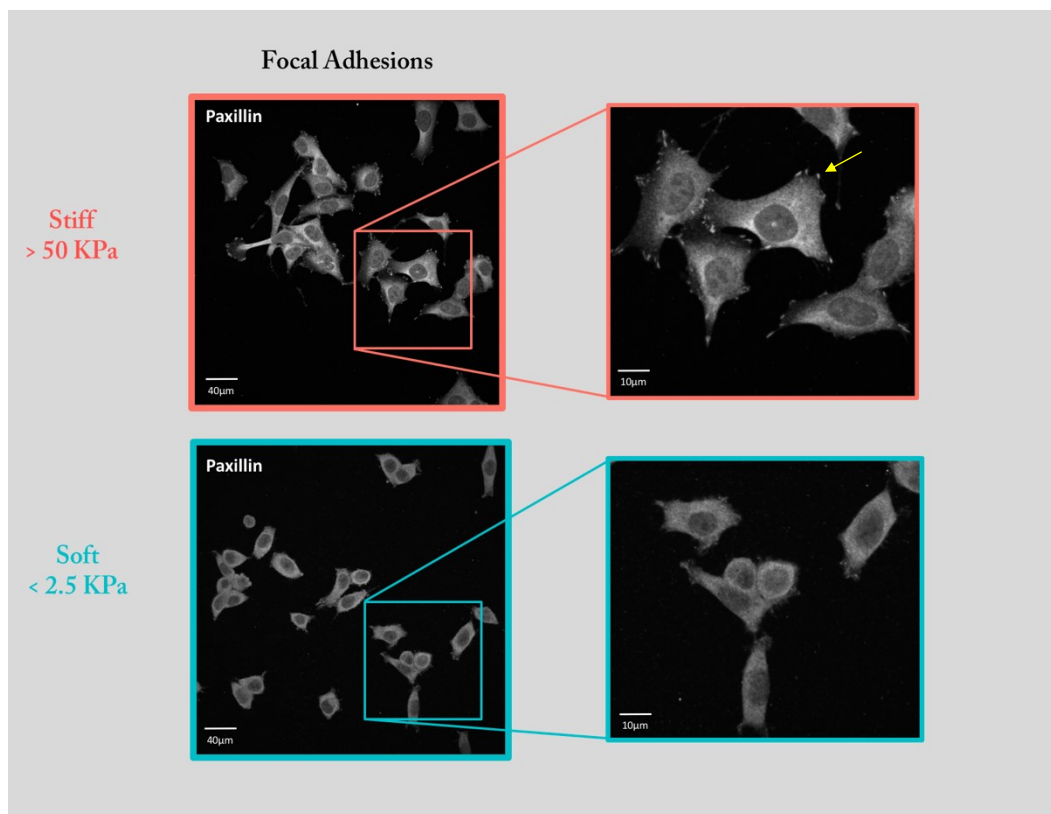


Figure 40. HeLa-H2B cultured on wide-range hydrogels and stained for cells paxillin protein which is expressed at FAs. First row images correspond to cells located at stiffest region of the gradient (>50 KPa) and second row images correspond to cells located at softest region of the gradient (<2.5 KPa). Yellow arrow indicates a visible FA.

5. DISCUSSION

The ECM that surrounds cells within the body is an important source of chemical and mechanical cues that influence different cellular processes (e.g., proliferation, differentiation and migration) and tissue homeostasis. Importantly, during pathological conditions the biochemical and mechanical properties of this complex niche where cells reside, can be considerably altered and lead to abnormal cell behaviour. For instance, the ECM stiffening produced by high and compact matrix deposition from altered fibroblasts has been elucidated as a critical factor in cancer progression (Acerbi et al., 2015; Butcher et al., 2009; Discher et al., 2005).

In order to investigate the effect of these mechanical cues on cells, PA-based hydrogels are commonly used as culture systems in many laboratories. However, most of the well-established protocols exist for the fabrication of hydrogels with a uniform stiffness (constant E). These hydrogels, although informative, poorly resemble the ECM stiffness heterogeneity observed *in vivo*, especially during some pathological conditions. To better understand the cellular processes involved in cell response to heterogeneous substrate stiffness (variable E), different methods have been developed for the generation of gradient stiffness PA-based hydrogels. These culture systems have their specific advantages and limitations, but overall, they are either difficult to reproduce or lack the possibility to know the stiffness to which cells are exposed without using AFM.

The first aim of the current thesis was to set up a methodology for the fabrication of PA-based hydrogels containing: (1) a gradient of stiffness and (2) a gradient of an indirect measure which could be correlated with the stiffness. The method required to be easily reproducible at any laboratory, low-cost, time-efficient and robust. Also, the generated hydrogel should be thin enough to allow the observation with high-resolution imaging.

Section 3.1 of materials and methods in this thesis provides detailed protocols for the fabrication of two different rigidity gradients: a wide range which spans from 2 KPa to 60 KPa and a narrow range which spans from 0.5 KPa to 22 KPa. The methodology used to create the stiffness gradient is based on a previous approach (Lo et al., 2000), specifically tailored towards fibroblast directional migration towards increased stiffness or “durotaxis”, with the incorporation of a few significant changes that better adapt to the laboratory needs. In contrast to Lo et al., the fabrication of our gradient hydrogels is carried out on a cell culture dish with thin (#1) glass-bottom well of high optical quality. In comparison with the original methodology, this petri dish facilitates the manipulation

of the hydrogels after polymerization and the glass thickness makes it suitable for a variety of microscopy techniques including high resolution. The current hydrogels can be easily fabricated in any laboratory without the need of specific equipment and at low-cost while others, such as photopolymerization methods (section 1.4.2), require specialized equipment/conditions and a tight control of many parameters that could easily lead to an erroneous stiffness gradient. At the same time, our method has proven to be time-efficient, being the fabrication time for one batch of hydrogels (5 hydrogels) of approximately 3 hours and the success ratio of four good-quality hydrogels out of the five. In contrast, when trying to replicate in the lab the method developed by Koser et al., we found it laborious and with poor reproducibility.

Except for the methods developed by Lo et.al. and Koser et al., most of the described methods lack an indirect measure that allows to infer the hydrogel stiffness without the need of using AFM (section 1.4.2). Koser et.al. added fluorescein in one of the PA solutions and determined the correlation between fluorescence intensity and stiffness, concluding a linear correlation between both. In our methodology, in contrast to Koser et.al., and similarly to Lo et.al, fluorescently labelled beads were embedded within one of the PA solutions before polymerization. However, while the aim of Lo et.al. was to simply differentiate between the stiff and soft part of the hydrogel, we went one step further and aimed to produce a gradient of beads that, if correlation existed, could be used as an indirect measure to know the stiffness at any point of the gel without the need of using AFM. Although we could have opted to use fluorescein as a means to measure stiffness, we believe that using density of beads is a more reliable measurement as the fluorescence intensity can hardly be influenced by bleaching and the microscope modality used.

Regarding the physical properties of the produced hydrogels, they are translucent and round with a diameter of 14 mm. One of the main advantages is their thickness, ranging from 80 to 100 μm , which together with the thin glass-bottom of the petri dish, makes them compatible with high-resolution imaging or for imaging live-cell dynamics. The distribution of the beads within the hydrogels shows three differentiated regions (*Figure 23*). The region containing the gradient of beads is displayed within an area of approximately 6 mm (W) x 2 mm (H) located in the middle-upper part of the gel. The gradient region is considerably small related to the total gel area. This is one of the main limitations of our methodology, as only cells located within this area can provide information on gradual mechanoresponse to the stiffness gradient. The reason for this

limitation is the approach that was used to create the gradient. The mixing between two adjacent drops by covering them with a coverslip can only achieve a limited distance of diffusion while in other methods, such as photopolymerization or two-layers polymerization, the methodology allows for a more controlled gradient generation and results in a bigger gradient area.

Another important characteristic that needs to be taken into account is that the hydrogel surface is slightly tilted towards the soft region of the hydrogel. This can be an issue when imaging cells, especially during the automatic acquisition of a big area. The tilted condition was less prominent in the wide-range than in the narrow-range hydrogels. The reason for this is thought to be related to the different physical properties associated to each solution of the PA mixture (soft region of the wide-range hydrogels was stiffer than the soft region of the narrow). Although this issue has not been entirely solved, it can be minimized by using a completely horizontal surface for the fabrication of the hydrogel.

The second aim of the current thesis was to generate the best fitting curve between stiffness and bead density, and to determine if there is a correlation between both parameters. Results shown in section 4.2 for each fabricated type of hydrogel, wide and narrow, confirm that the hydrogels contain a gradient of stiffness and that the stiffness values span between the expected rigidity ranges (approximately 2 KPa to 60 KPa for the wide range and 0.5 KPa to 22 KPa for the narrow range).

In addition, the analyses demonstrate that, in both instances, the AFM-defined stiffness correlates with the density of beads. The correlation curve obtained for the wide-range hydrogels (2 KPa to 60 KPa) shows a linear relationship in the middle ranges, whereas at both extremes, significant stiffness changes correspond with very little changes in bead density (*Figure 26*). The best fitting model describing this behaviour is the Logit function, which reflects the saturation of beads at both stiffness extremes of the curve. In contrast, the curve generated for the narrow-range hydrogels (0.5 KPa to 22 KPa) appears to exhibit a linear correlation between stiffness and bead density, and can be best described by a linear function (*Figure 29*). Although both curves exhibit a linear relationship in the middle ranges of the gradient, it is unknown why the wide-range model shows saturation at the extremes. Further investigation would be necessary to shed some light on this topic.

When comparing the SE of the averaged bead density for each data point of the curves (horizontal error bar), it can be observed that these values are smaller in the narrow than in the wide range. The implementation carried out during the fabrication of the narrow-

range hydrogels, using a gridded glass-bottom petri dish instead of a plain glass-bottom petri dish, was the only change incorporated. This demonstrates that adding a gridded glass-bottom petri dish improves the quality of the methodology, as expected. The incorporation of the new mould facilitates the localization of the same area under both microscopes (SDCM and AFM), reducing the co-localization uncertainty of the previously used mould. Despite the improvement, the resolution of the SDCM is still much lower than the AFM (each stiffness point measured by the AFM corresponds to a much smaller area than the image acquired with the SDCM). This means that it is not possible to precisely co-localize both measurements and, therefore, there is still the need of averaging the 4 closest images of beads to the AFM measurement. In conclusion, the incorporation of the gridded glass-bottom petri dish improves the co-localization accuracy, is less prone to human error and consequently leads to a more robust methodology. However, the co-localization accuracy between both measurements is not completely precise and it could be partly improved by using gridded glass-bottom petri dish with even a smaller grid.

The possibility to apply the methodology to produce different rigidity gradients probes the flexibility of the technique. By modifying the PA composition of the starting premix solution, it is possible to generate the desire gradient range. In spite of this, because a different correlation curve model could be generated depending on the original PA mix, it would be necessary to carry out the protocol for the generation of a new correlation curve unless using one of the two presented gradients in this master's thesis.

All in all, the generated correlation curves demonstrate the positive correlation between bead density and stiffness. By using the corresponding equations (*Equation 3 and Equation 5*), researchers should be able to infer the stiffness in every spot within both types of hydrogels by simply measuring the density of beads, replacing the need of using AFM by a more accessible microscopy technique such as confocal microscopy.

Finally, the third aim of this thesis was to numerically validate the generated wide-range correlation curve (2 KPa to 60 KPa) and to assess the biological applicability of this gradient hydrogels by testing cancer cells mechanoresponse to stiffness.

The numerical validation of the wide-range hydrogels was carried out by comparing the real stiffness (ground truth) from one wide-range hydrogel, measured by AFM at random locations across the whole stiffness range, to the calculated stiffness. The stiffness calculation derives from inserting the corresponding bead density at those random

locations into the wide-range equation. The results shown in section 4.3.1 (*Figure 32*) show that all the calculated stiffness values fall within the CI of the standard curve. Although more replicas would be needed to further confirm this validation, the current results are promising and show that the generated correlation curve can be used to infer the stiffness from the density of beads with enough accuracy for most use cases.

To validate the biological applicability of the wide-range hydrogels (2 KPa to 60 KPa), three different mechanoresponsive aspects of HeLa H2B-GFP cells to substrate stiffness were monitored: subcellular localization of mechanoresponsive proteins (YAP/TAZ, Oct1 and MATL), cell morphology (cell area and circularity) and expression of FAs (number and size). The initial idea was to monitor the gradual variation of these three aspects across the stiffness gradient, and try to identify stiffness threshold values of cell mechano-responsiveness. However, after seeding the cells on a few hydrogels, it was found that cells exhibited a stiff phenotype already at approximately 7 KPa where only a few beads were present and exhibited a soft phenotype at softer values where few or no beads were present (*Figure 20*). These results revealed that the wide-range hydrogels have a very steep stiffness gradient and the stiffness range was too wide to track gradual cell changes at softer regions of the gradient. Although this limits the applicability to monitor progressive changes in cell rigidity sensing, at least with respect to processes regulating the aspects under this study and associated to this type of cells, this steep gradient could be useful to monitor cell processes that happen at stiffer values.

Nonetheless, the biological functionality of this wide-range hydrogels was still carried out. Cells located within the gradient were avoided in the analysis, and the three mechanoresponsive aspects were compared between cells located at the softest region of the gel (no beads) versus cells located at the stiffest part of the gel (high number of beads). YAP/TAZ subcellular localization has been previously reported to undergo cytoplasmic-to-nuclear in response to increasing stiffness. The same behaviour was expected for Oct1 and MASTL, the two other mechano-mediators which are under investigation in this laboratory. Indeed, the results shown in section 4.3.2 (*Table 2*) for the wide-range hydrogels confirm that the subcellular localization of YAP/TAZ, Oct1 and MASTL is predominantly cytoplasmic at the softest region of the gel (<2.5 KPa) and the localization becomes predominantly nuclear at the stiffest regions of the gel (<50 KPa). Regarding cell morphology, cells located in the stiffest region were bigger and less rounded than those located in the softest region as expected. Finally, the FAs were visually assessed to confirm that cells located in the stiffest part of the gel exhibited higher number and bigger

size of these mechanosensing structures than those located on the softest region. Altogether, it has been confirmed that cells mechanoreponse to substrate stiffness, at both extremes of the gradient corresponds to the expected cell behaviour (*Figure 10*), thus, demonstrating that the wide-range hydrogels can be used as a culture system to dissect the mechanosensitive scope of cells.

The narrow-range hydrogels (0.5 KPa to 22 KPa) were generated in order to create a softer stiffness range that would overcome the explained limitations of the wide-range hydrogels, and consequently would allow to better track gradual changes in mechanoreponsiveness of cells under study as well as others cell types with similar response to stiffness. As previously mentioned, this thesis provides the protocol for the fabrication of narrow-range gradient hydrogels and the corresponding correlation curve between stiffness and bead density. The obtained results are promising, nonetheless the numerical and biological validation of this narrow-range hydrogels are outside the scope of this thesis and future experiments would be required to validate their applicability.

6. CONCLUSIONS

6.1. Conclusions

In this Master's Thesis, two PA-based stiffness gradient hydrogels have been developed, a wide-range hydrogel with a stiffness gradient ranging from 2 KPa to 60 KPa and a narrow-range hydrogel ranging from 0.5 KPa to 22 KPa. On one hand, the technique used for the fabrication has been demonstrated to be flexible, cost-effective, simple and robust. On the other hand, the fabricated hydrogels are very thin, making them compatible for high-resolution imaging or for live-cell dynamics. By using bead density as an indirect measure for hydrogel stiffness, we have been able to determine that there is a correlation between both parameters, providing the corresponding equation which allows to know the stiffness at a certain location of the hydrogel by simply calculating the density of beads at this same location without the need of using AFM. We have also shown that within a 2 KPa - 60 KPa range, HeLa cells behave as expected in response to stiffness. Altogether, concluding that these hydrogels could be a simple and reductionist model to dissect the mechanosensitive response of cells to stiffness.

6.2. Future work

As one of the main sources of uncertainty regarding the generation of the correlation curves comes from the resolution difference that exists between the AFM and the SDCM, an important improvement would be to incorporate a glass-bottom petri dish with a smaller grid than the one used in the current thesis. This would allow to more precisely identify the same location at both devices and to reduce the accuracy error.

The next steps to improve the methodology would include to use more replicas of the wide-range hydrogels to confirm the numerical validation of the generated correlation curve. The correlation curve of the narrow-range hydrogels would require a complete numerical validation. Also, a biological validation would be required to confirm that it is possible to use these gels with a softer stiffness range to study cells' gradual mechanoresponse to stiffness, for instance, to determine stiffness-dependent biological thresholds as it could be the precise threshold for a complete nuclear translocation of YAP/TAZ of HeLa cells.

ABBREVIATIONS

AFM	Atomic force microscopy
APS	Ammonium persulfate
<i>E</i>	Young's modulus
ECM	Extracellular matrix
FA	Focal adhesion
HeLa	Human cervical adenocarcinoma cell
IC	Interval of confidence
GFP	green fluorescent protein
Mean	M
N	Newton
Pa	Pascals
PA	Polyacrylamide
PBS	Phosphate-buffered saline
ROI	Region of interest
RT	Room temperature
SDCM	Spinning-disk confocal microscopy
SE	Standard error
TEMED	Tetramethylethylenediamine
UV	Ultraviolet

REFERENCES

- Acerbi, I., Cassereau, L., Dean, I., Shi, Q., Au, A., Park, C., ... Weaver, V. M. (2015). Human breast cancer invasion and aggression correlates with ECM stiffening and immune cell infiltration. *Integrative Biology*, 7(10), 1120–1134.
- Ahearne, M., Yang, Y., & Liu, K. (2008). Mechanical Characterisation of Hydrogels for Tissue Engineering Applications.
- Alberts, B., Johnson, A., Lewis, J., Raff, M., Roberts, K., & Walter, P. (2007). *Molecular biology of the cell: Reference edition*. Garland Science.
- Attieh, Y., & Matic, D. (2016). European Journal of Cell Biology The hallmarks of CAFs in cancer invasion. *European Journal of Cell Biology*, 95(11), 493–502. <https://doi.org/10.1016/j.ejcb.2016.07.004>
- Butcher, D. T., Alliston, T., & Weaver, V. M. (2009). A tense situation: forcing tumour progression. *Nature Reviews Cancer*, 9(2), 108–122.
- Caliari, S. R., & Burdick, J. A. (2016). A practical guide to hydrogels for cell culture. *Nature Methods*, 13(5), 405.
- Chen, C. S. (2008). Mechanotransduction--a field pulling together? *Journal of Cell Science*, 121(20), 3285–3292.
- Chin, L., Xia, Y., Discher, D. E., & Janmey, P. A. (2016). Mechanotransduction in cancer. *Current Opinion in Chemical Engineering*, 11, 77–84.
- Cox, T. R., & Ertler, J. T. (2011). Remodeling and homeostasis of the extracellular matrix: implications for fibrotic diseases and cancer. *Disease Models & Mechanisms*, 4(2), 165–178.
- Discher, D. E., Janmey, P., & Wang, Y. (2005). Tissue cells feel and respond to the stiffness of their substrate. *Science*, 310(5751), 1139–1143.
- Discher, D. E., Mooney, D. J., & Zandstra, P. W. (2009). Growth factors, matrices, and forces combine and control stem cells. *Science*, 324(5935), 1673–1677.
- Dupont, S. (2016). Role of YAP/TAZ in cell-matrix adhesion-mediated signalling and mechanotransduction. *Experimental Cell Research*, 343(1), 42–53.
- Dupont, S., Morsut, L., Aragona, M., Enzo, E., Giulitti, S., Cordenonsi, M., ... others. (2011). Role of YAP/TAZ in mechanotransduction. *Nature*, 474(7350), 179.
- Elkrief, L., Rautou, P.-E., Ronot, M., Lambert, S., Dioguardi Burgio, M., Francoz, C., ... others. (2014). Prospective comparison of spleen and liver stiffness by using shear-wave and transient elastography for detection of portal hypertension in cirrhosis. *Radiology*, 275(2), 589–598.
- Elosegui-artola, A., Andreu, I., Beedle, A. E. M., Navajas, D., Garcia-manyes, S.,

- Elosegui-artola, A., ... Kosmalska, A. J. (2017). Force Triggers YAP Nuclear Entry by Regulating Transport across Nuclear Pores. *Cell*, 1–14.
<https://doi.org/10.1016/j.cell.2017.10.008>
- Elosegui-Artola, A., Oria, R., Chen, Y., Kosmalska, A., Pérez-González, C., Castro, N., ... Roca-Cusachs, P. (2016). Mechanical regulation of a molecular clutch defines force transmission and transduction in response to matrix rigidity. *Nature Cell Biology*, 18(5), 540.
- Engler, A. J., Richert, L., Wong, J. Y., Picart, C., & Discher, D. E. (2004). Surface probe measurements of the elasticity of sectioned tissue, thin gels and polyelectrolyte multilayer films: correlations between substrate stiffness and cell adhesion. *Surface Science*, 570(1-2), 142–154.
- Hadden, W. J., Young, J. L., Holle, A. W., McFetridge, M. L., Kim, D. Y., Wijesinghe, P., ... others. (2017). Stem cell migration and mechanotransduction on linear stiffness gradient hydrogels. *Proceedings of the National Academy of Sciences*, 114(22), 5647–5652.
- Hamidi, H., & Ivaska, J. (2018). Every step of the way: integrins in cancer progression and metastasis. *Nature Reviews Cancer*, 1.
- Handorf, A. M., Zhou, Y., Halanski, M. A., & Li, W.-J. (2015). Tissue stiffness dictates development, homeostasis, and disease progression. *Organogenesis*, 11(1), 1–15.
- Hay, E. D. (2013). *Cell biology of extracellular matrix*. Springer Science & Business Media.
- Hertz, H. (1881). On the contact of elastic solids. *Z. Reine Angew. Mathematik*, 92, 156–171.
- Horton, E. R., Byron, A., Askari, J. A., Ng, D. H. J., Millon-Frémillon, A., Robertson, J., ... others. (2015). Definition of a consensus integrin adhesome and its dynamics during adhesion complex assembly and disassembly. *Nature Cell Biology*, 17(12), 1577.
- Humphrey, J. D., Dufresne, E. R., & Schwartz, M. A. (2014). Mechanotransduction and extracellular matrix homeostasis. *Nature Reviews Molecular Cell Biology*, 15(12), 802.
- Hutter, J. L., & Bechhoefer, J. (1993). Calibration of atomic-force microscope tips. *Review of Scientific Instruments*, 64(7), 1868–1873.
- Iskratsch, T., Wolfenson, H., & Sheetz, M. P. (2014). Appreciating force and shape—the rise of mechanotransduction in cell biology. *Nature Reviews Molecular Cell Biology*, 15(12), 825.
- JPK instruments. (2012). *NanoWizard AFM Handbook*.
- Kanchanawong, P., Shtengel, G., Pasapera, A. M., Ramko, E. B., Davidson, M. W.,

- Hess, H. F., & Waterman, C. M. (2010). Nanoscale architecture of integrin-based cell adhesions. *Nature*, *468*(7323), 580.
- Kass, L., Erler, J. T., Dembo, M., & Weaver, V. M. (2007). Mammary epithelial cell: influence of extracellular matrix composition and organization during development and tumorigenesis. *The International Journal of Biochemistry & Cell Biology*, *39*(11), 1987–1994.
- Kaukonen, R., Mai, A., Georgiadou, M., Saari, M., De Franceschi, N., Betz, T., ... others. (2016). Normal stroma suppresses cancer cell proliferation via mechanosensitive regulation of JMJD1a-mediated transcription. *Nature Communications*, *7*, 12237.
- Kechagia, J. Z., Ivaska, J., & Roca-Cusachs, P. (2019). Integrins as biomechanical sensors of the microenvironment. *Nature Reviews Molecular Cell Biology*, *1*.
- Khalili, A., & Ahmad, M. (2015). A review of cell adhesion studies for biomedical and biological applications. *International Journal of Molecular Sciences*, *16*(8), 18149–18184.
- Khatiwala, C. B., Peyton, S. R., & Putnam, A. J. (2006). Intrinsic mechanical properties of the extracellular matrix affect the behavior of pre-osteoblastic MC3T3-E1 cells. *American Journal of Physiology-Cell Physiology*, *290*(6), C1640–C1650.
- Koser, D. E., Thompson, A. J., Foster, S. K., Dwivedy, A., Pillai, E. K., Sheridan, G. K., ... others. (2016). Mechanosensing is critical for axon growth in the developing brain. *Nature Neuroscience*, *19*(12), 1592.
- Lampi, M. C., & Reinhart-King, C. A. (2018). Targeting extracellular matrix stiffness to attenuate disease: From molecular mechanisms to clinical trials. *Science Translational Medicine*, *10*(422), eaao0475.
- Larsen, M., Artym, V. V., Green, J. A., & Yamada, K. M. (2006). The matrix reorganized: extracellular matrix remodeling and integrin signaling. *Current Opinion in Cell Biology*, *18*(5), 463–471.
- Liu, Z., & Vunjak-Novakovic, G. (2016). Modeling tumor microenvironments using custom-designed biomaterial scaffolds. *Current Opinion in Chemical Engineering*, *11*, 94–105.
- Lo, C.-M., Wang, H.-B., Dembo, M., & Wang, Y. (2000). Cell movement is guided by the rigidity of the substrate. *Biophysical Journal*, *79*(1), 144–152.
- Mao, A. S., Shin, J.-W., & Mooney, D. J. (2016). Effects of substrate stiffness and cell-cell contact on mesenchymal stem cell differentiation. *Biomaterials*, *98*, 184–191.
- Moffat, K. L., Sun, W.-H. S., Pena, P. E., Chahine, N. O., Doty, S. B., Ateshian, G. A., ... Lu, H. H. (2008). Characterization of the structure--function relationship at the ligament-to-bone interface. *Proceedings of the National Academy of Sciences*,

105(23), 7947–7952.

- Muhamed, I., Chowdhury, F., & Maruthamuthu, V. (2017). Biophysical Tools to Study Cellular Mechanotransduction. *Bioengineering*, 4(1), 12.
- Nematbakhsh, Y., & Lim, C. T. (2015). 10 Micro- and nanotools to probe cancer cell mechanics and mechanobiology. *Integrative Mechanobiology: Micro- and Nano-Techniques in Cell Mechanobiology*, 169.
- Neumann, T. (2008). Determining the elastic modulus of biological samples using atomic force microscopy. *JKP Instruments Application Report*, 1–9.
- Panciera, T., Azzolin, L., Cordenonsi, M., & Piccolo, S. (2017). Mechanobiology of YAP and TAZ in physiology and disease. *Nature Reviews Molecular Cell Biology*, 18(12), 758.
- Paszek, M. J., Zahir, N., Johnson, K. R., Lakins, J. N., Rozenberg, G. I., Gefen, A., ... others. (2005). Tensional homeostasis and the malignant phenotype. *Cancer Cell*, 8(3), 241–254.
- Pickup, M. W., Mouw, J. K., & Weaver, V. M. (2014). The extracellular matrix modulates the hallmarks of cancer. *EMBO Reports*, e201439246.
- Plotnikov, S. V, Pasapera, A. M., Sabass, B., & Waterman, C. M. (2012). Force fluctuations within focal adhesions mediate ECM-rigidity sensing to guide directed cell migration. *Cell*, 151(7), 1513–1527.
- Provenzano, P. P., Inman, D. R., Eliceiri, K. W., & Keely, P. J. (2009). Matrix density-induced mechanoregulation of breast cell phenotype, signaling and gene expression through a FAK--ERK linkage. *Oncogene*, 28(49), 4326.
- Rehfeldt, F., Engler, A. J., Eckhardt, A., Ahmed, F., & Discher, D. E. (2007). Cell responses to the mechanochemical microenvironment—implications for regenerative medicine and drug delivery. *Advanced Drug Delivery Reviews*, 59(13), 1329–1339.
- Richter, C.-P., Emadi, G., Getnick, G., Quesnel, A., & Dallos, P. (2007). Tectorial membrane stiffness gradients. *Biophysical Journal*, 93(6), 2265–2276.
- Schindelin, J., Arganda-Carreras, I., Frise, E., Kaynig, V., Longair, M., Pietzsch, T., ... others. (2012). Fiji: an open-source platform for biological-image analysis. *Nature Methods*, 9(7), 676.
- Sun, Z., Guo, S. S., & Fässler, R. (2016). Integrin-mediated mechanotransduction. *J Cell Biol*, 215(4), 445–456.
- Sunyer, R., Jin, A. J., Nossal, R., & Sackett, D. L. (2012). Fabrication of hydrogels with steep stiffness gradients for studying cell mechanical response. *PLoS One*, 7(10), e46107.

- Takuma, Y., Nouse, K., Morimoto, Y., Tomokuni, J., Sahara, A., Takabatake, H., ... Yamamoto, H. (2015). Portal hypertension in patients with liver cirrhosis: diagnostic accuracy of spleen stiffness. *Radiology*, *279*(2), 609–619.
- Tse, J. R., & Engler, A. J. (2010). Preparation of hydrogel substrates with tunable mechanical properties. *Current Protocols in Cell Biology*, 10–16.
- Vicente-Manzanares, M., Choi, C. K., & Horwitz, A. R. (2009). Integrins in cell migration--the actin connection. *Journal of Cell Science*, *122*(2), 199–206.
- Vining, K. H., & Mooney, D. J. (2017). Mechanical forces direct stem cell behaviour in development and regeneration. *Nature Reviews Molecular Cell Biology*, *18*(12), 728.
- Wang, N., Tytell, J. D., & Ingber, D. E. (2009). Mechanotransduction at a distance: mechanically coupling the extracellular matrix with the nucleus. *Nature Reviews Molecular Cell Biology*, *10*(1), 75.
- Waterman, C. (2014). Force Fluctuations within Focal Adhesions Mediate ECM-Rigidity Sensing to Guide Directed Cell Migration. In *APS Meeting Abstracts*.
- Wong, J. Y., Leach, J. B., & Brown, X. Q. (2004). Balance of chemistry, topography, and mechanics at the cell--biomaterial interface: issues and challenges for assessing the role of substrate mechanics on cell response. *Surface Science*, *570*(1-2), 119–133.
- Wong, J. Y., Velasco, A., Rajagopalan, P., & Pham, Q. (2003). Directed movement of vascular smooth muscle cells on gradient-compliant hydrogels. *Langmuir*, *19*(5), 1908–1913.
- Xia, T., Liu, W., & Yang, L. (2017). A review of gradient stiffness hydrogels used in tissue engineering and regenerative medicine. *Journal of Biomedical Materials Research Part A*, *105*(6), 1799–1812.
- Yeung, T., Georges, P. C., Flanagan, L. A., Marg, B., Ortiz, M., Funaki, M., ... Janmey, P. A. (2005). Effects of substrate stiffness on cell morphology, cytoskeletal structure, and adhesion. *Cell Motility and the Cytoskeleton*, *60*(1), 24–34.